

**A 6-BEAM COMBINER USING SUPERIMPOSED VOLUME INDEX
HOLOGRAPHIC GRATINGS**

A Thesis

by

HO NAM YUM

Submitted to the Office of Graduate Studies of
Texas A&M University
in partial fulfillment of the requirements for the degree of

MASTER OF SCIENCE

August 2004

Major Subject: Electrical Engineering

**A 6-BEAM COMBINER USING SUPERIMPOSED VOLUME INDEX
HOLOGRAPHIC GRATINGS**

A Thesis

by

HO NAM YUM

Submitted to Texas A&M University
in partial fulfillment of the requirements
for the degree of

MASTER OF SCIENCE

Approved as to style and content by:

Philip Hemmer
(Chair of Committee)

Henry F. Taylor
(Member)

Gerard Cote
(Member)

Prasad Enjeti
(Member)

Chanan Singh
(Head of Department)

August 2004

Major Subject: Electrical Engineering

ABSTRACT

A 6-beam Combiner Using Superimposed Volume Index Holographic Gratings.

(August 2004)

Ho Nam Yum, B.S., Yonsei University;

Chair of Advisory Committee: Dr. Philip Hemmer

In this thesis, a 6-beam combiner using multiplexed holograms in dye-doped polymer is investigated. It is realized by recording six superimposed holographic gratings, which show uniform diffraction efficiency. The coupled wave theory for N superimposed gratings is more generalized and is used to analyze the amplitudes of diffracted waves in three different boundary conditions.

Multiple-ring diffracted beam analysis is proposed to determine the dynamic range of a holographic material. The $M/\#$ is evaluated by recording a single hologram and counting the number of ring patterns in the diffracted beam. This analysis is extended to assess the equalized grating strength of N superimposed holograms. Six holograms with the equalized grating strength which can be assigned within the dynamic range of our material and show maximum diffraction efficiency are recorded.

The phase locking of five beams to one reference beam is performed using PZT controller. The designs of lock-in amplifier, ramp generator and servo using commercial chips are demonstrated. The readout set-up used to split one single beam into six coherent copies is presented. The function of each part of the PZT controller in the readout set-up is discussed in detail.

The intensity profile of an N-beam combiner is investigated by varying the phase angle between adjacent input waves. The entire solution which describes the amplitude of a combined beam is derived from generalized coupled wave theory. A simplified experimental set-up without a complicated PZT controller is demonstrated using a plano-convex lens. In order to provide six coherent light sources in future work, the injection locking of a single laser diode to the master laser diode is performed. An expected read-out setup is proposed to carry out both the achievement of six coherent sources and a 6 beam combination.

DEDICATION

To my parents and lovely sister

ACKNOWLEDGEMENTS

I would like to thank Dr. Philip Hemmer, my academic advisor, for his continuous support, mentoring and guidance, and especially for his sincerity and patience during my research. I would like to acknowledge the efforts and concerns of my committee: Dr. Henry F. Taylor, Dr. Prasad Enjeti, Dr. Gerard Cote.

TABLE OF CONTENTS

	Page
ABSTRACT.....	iii
DEDICATION.....	v
ACKNOWLEDGEMENTS.....	vi
TABLE OF CONTENTS.....	vii
LIST OF FIGURES.....	ix
LIST OF TABLES.....	xii
I. INTRODUCTION.....	1
II. THEORETICAL BACKGROUND FOR A MULTI-BEAM COMBINER.....	4
A. Coupled wave analysis for multiple thick holographic gratings.....	4
B. Simulation results for multiple thick holographic gratings in three different modes.....	10
III. CHARACTERIZATION OF THE RECORDING DYNAMICS OF A HOLOGRAPHIC MATERIAL AND RECORDING OF 6 HOLOGRAMS WITH EQUALIZED GRATING STRENGTHS.....	19
A. Introduction to a holographic material and Mechanism of hologram formation in a photopolymer material.....	19
B. Demonstration of a simple technique for determining the $M/\#$ a holographic substrate using a single exposure.....	20
C. Exposure schedule and holographic recording set-up using the angular multiplexing.....	29
D. Determination of equalized grating strength analyzing output waves in the beam splitter mode.....	33

	Page
IV. BEAM COMBINATION USING SERVOS AND LOCK-IN AMPLIFIERS.....	42
A. Design of lock-in amplifier using an Analog Devices' AD630AD.....	42
B. Beam combination using PZT controller and multiplexed six holograms....	43
V. BEAM COMBINATION USING PLANO CONVEX LENS AND EXPERIMENTAL PERFORMANCE OF THE INJECTION LOCKING FOR POTENTIAL READING SETUP.....	58
A. Investigation of the influence of phase angle variation between two input waves on the intensity of an output wave.....	58
B. Experimental demonstration of 6 beam combiner varying phase angle between adjacent waves.....	62
C. Frequency synchronization of diode lasers by injection locking.....	66
VI. CONCLUSIONS AND FUTURE WORK.....	69
REFERENCES.....	73
VITA.....	77

LIST OF FIGURES

	Page
Figure 1. Schematic illustration of the reconstruction of object waves illuminating on superimposed multiple gratings with a reference wave.....	5
Figure 2. Bragg matched diagram for multiple gratings.....	7
Figure 3. Angle relationships between in grating layers and x-z plane.....	8
Figure 4. Relative efficiencies η/η_0 for the splitter mode as a function of equal grating strengths normalized by $\nu_0=\pi/2$, the grating strength which gives a single hologram 100% diffraction efficiency. Peak efficiency of $\eta_0 =1$	13
Figure 5. Relative efficiencies η/η_0 for the combiner mode are plotted. All input beams are in phase. Peak efficiency of $\eta_0 =1$	14
Figure 6. Relative efficiencies η/η_0 for the cross-coupled mode are plotted. One input wave in the direction of beam S_3 is illuminating the 6 gratings. Peak efficiency of $\eta_0 =1$	15
Figure 7. Relative efficiency η/η_0 for the cross coupled mode are plotted. Five input waves, S_1, S_2, S_4, S_5, S_6 are illuminating the six gratings. Peak efficiency of $\eta_0 =1$	16
Figure 8. Relative efficiency η/η_0 for six non-equal inputs in the beam combiner mode are plotted. Amplitude difference between adjacent two inputs set to three different values. (a) 0.16, (b) 0.1, (c) 0.05.....	18
Figure 9. Mechanism of hologram formation in a photopolymer system.....	20
Figure 10(a) Simulation results showing the evolution of diffracted pattern as a function of holographic exposure for an even Q ($m=5, n=0, \alpha=0$ in Eqn. (36)) value material with a plane wave read-out beam.....	26
Figure 10(b) Simulation result showing the diffracted pattern for an odd Q ($m=5, n=1, \alpha=0$ in Eqn. (36)) value material	

	Page
with a Gaussian read-out beam.....	27
Figure 11. Simulation results for the diffraction pattern for fractional Q with a plane wave read-out beam. (a). $m=5, n=0, \alpha=0.2$ in Eqn. (36) (b). $m=5, n=1, \alpha=0.2$ in Eqn. (36).....	27
Figure 12. Writing and Read-out Geometry.....	28
Figure 13. Angle multiplexing, in-plane.....	32
Figure 14. Experimental set-up for holographic recording using angular multiplexing.....	32
Figure 15. Efficiencies of output beams as a function of beam radius for four different center-equalized grating strength with a Gaussian read-out beam	36
Figure 16. Efficiencies of the transmitted beams of single holograms for four different grating strengths with a Gaussian read-out beam.....	37
Figure 17. Recording set-up with Nd-YAG laser using the angular multiplexing and Read-out with the identical laser.....	39
Figure 18. Lock-in amplifier detects the phase difference between two sinusoids identified as “Reference” and “Signal”.....	42
Figure 19. AD630 with external electronic components functions as demodulator followed by two stage of low pass filter.....	43
Figure 20. Experimental set-up for beam combining. BS: beam splitter, MR: mirror, NDF: neutral density filter.....	44
Figure 21. The fringe patterns by interference of each pair of beams. The number below the images notes the numbers of two input beams.....	46
Figure 22. Schematic diagrams of ramp generator and servo (a) Ramp generator using Harris’ ICL8038 (b) Servo combined with summing amplifier.....	48
Figure 23. Ramp and sinusoid signals scan and modulate laser intensity.	

	Page
Demodulator in lock-in amplifier is fed with the modulated signal.....	50
Figure 24. PZT controller consists of the circuits in Fig. 20, Fig. 21 and Fig. 18, and sine wave function generators.....	53
Figure 25. Calculated intensity of output wave in the direction of reference wave S_0 as a function of phase angle between adjacent input waves.....	60
Figure 26. Simulation results showing the intensity of output wave as a function of equalized grating strength, ν	61
Figure 27. The intensity of S_0 is plotted as a function of phase angle difference between adjacent waves for $\nu=0.23\pi$	62
Figure 28. Experimental setup for six beam combining with the 2 nd sample which has six superimposed gratings and functions as holographic beam combiner. The focal length of lens is 25cm.....	64
Figure 29. Intensity measured by photodetector in experimental setup as shown Fig. 28.....	65
Figure 30. Combined set-up for a two beam interferometer and injection locking.....	67
Figure 31. Image of the combined two beams captured by a CCD (a) without and (b) with optical feedback.....	67
Figure 32. Expected read-out setup using injection locking ML: master laser, SL: slave laser, FI: faraday isolator, Dashed line: Injected beams into slave lasers, Solid line: Coherent input beams from slave lasers.....	68

LIST OF TABLES

	Page
Table 1. Experimentally observed transmission and diffraction patterns for 3 different exposures. As one reaches the optimum limit for holographic exposure, the number of interference fringes visible in the diffracted reach a maximum.....	29
Table 2. Experimentally observed transmission and diffraction patterns for 4 superimposed gratings. The profiles show the relative efficiency η/η_0 , as a function of beam radius. (The unit of beam radius: μm , Peak efficiency of $\eta_0=1$).....	40
Table 3. Experimentally observed transmission and diffraction patterns for 6 superimposed gratings. The profiles show the relative efficiency η/η_0 , as a function of beam radius. (The unit of beam radius: μm , Peak efficiency of $\eta_0=1$)	41
Table 4. (a) Experimental conditions for the combination of each pair of beams. Scan range and modulation frequency are determined by PZT response. The scan range is wide enough to obtain two or three peaks And the modulation frequency is set within PZT resonance frequency range (b) The intensity of each input wave is equalized by neutral density filter as shown in Fig. 24(c). The intensity of each diffracted wave is measured by a photodetector.....	57

I. INTRODUCTION

Various industrial and technological fields require inexpensive high power lasers. Low power lasers are much cheaper per watt than high power lasers. Therefore, if one can combine multiple cheap low power lasers into a single beam, the cost is lower. A holographic beam combiner is one method to combine the beams.

We combine multiple beams by incoherently superimposed index gratings fabricated in lossless holographic media. Generalized coupled wave theory describes all diffracted waves in the Bragg-matched or mismatched condition, and lossy or lossless media. Most of the notations and conditions assumed in our works are identical to those by Kogelnik [1]. Simulated results for the efficiencies of output waves based on four different boundary conditions are presented.

A Beam combiner is demonstrated by using two different methods. In the first, a Lock-in amplifier is used to lock the phases of five input waves to that of one reference wave. The function of lock-in amplifiers is to detect very small AC signal (a few nanovolts) buried in dominant noise and produce derivative for locking to peak [2], [3]. Commercial chips can be used to design lock-in amplifiers [3] and waveform generators [4]. Lock-in amplifier and ramp generator are implemented using Analog Device's AD630AD and Harris' ICL8038 respectively. The design of system to drive Piezo materials is performed by utilizing lock-in amplifiers, ramp generators, servos and oscillators. The locking process of lock-in output to servo's reference eventually results in keeping six input waves in phase and maximizing the intensity of the six combined

This thesis follows the style and format of IEEE *Transactions on Antennas and Propagation*.

beams.

In the second method, a simplified way to characterize a beam combiner using a plano-convex lens and mirrors is demonstrated. This simplified method make possible to combine six beams without the complicated PZT controller systems. The variation of phase angle between adjacent input waves causes N-beam combiner to produce intensity variations that are analogous to multiple interferences in Fabry-Perot. The number of input waves contributing to beam combination determines the finesse of the intensity profile. For the case that all input waves are in-phase, and the grating strength is equal for each wave, the intensity is at peak value. Comparing the observed peak height to theory gives a simple technique to assess the quality of the beam combiner.

The frequency synchronization of laser diodes by injection locking is another essential step to realize a high power coherent beam combiner. The phases of input lasers are locked to that of one reference laser so that the input lasers start behaving coherently. Injection locking [5], [6], [7] for two light sources, is performed. This experimental demonstration is a primary set-up for future work in which six coherent light sources will be obtained.

To characterize the dynamic range performance of a holographic medium [8], $M/\#$ was proposed. This quantity is an important factor which estimates the storage density and diffraction efficiency for holographic data storage and beam combiners [9], [10], [11], [12]. Moreover, one needs $M/\#$ in order to determine how many beams can be combined with a given holographic material.

$M/\#$ can be experimentally evaluated by multiplexing many holograms in the same location because subsequent exposure exhausts the materials response [8], [9], [13], [14]. F.H. Mok recorded 1000 holograms to measure $M/\#$ [8]. In our experiment, we record a single hologram with long enough exposure to saturate the holographic material. Multiple ring patterns appear in diffracted image. $M/\#$ is determined by the number of rings and the brightness on the center of the image.

II. THEORETICAL BACKGROUND FOR A MULTI-BEAM COMBINER

A. Coupled-Wave Analysis for Multiple Thick Holographic Gratings

The coupled wave theory for thick hologram gratings, established by Kogelnik [1] described the diffraction efficiency of a thick hologram and provided solutions for the amplitudes of signal and reference wave. Thick hologram gratings cause energy interchange between the incoming reference wave and the outgoing signal wave at or near the Bragg angle. S. K. Case [15] developed the coupled wave theory into the analysis of the Bragg-matched diffraction for two sets of incoherently superimposed gratings. He determined the efficiencies of diffracted waves within a refractive-index-modulated lossless holographic material and showed an experimental verification for two different modes such as the beam splitter and combiner. R. Magnusson [16] considered the first and higher diffracted orders in gratings with arbitrary shapes and all possible incident angles including the Bragg angle. Further more equations for the efficiencies of higher order diffracted beams, which can be significant in holographic gratings with large refractive index modulations ($n_1 \approx 10^{-3} \sim 10^{-1}$), were obtained by the coupled wave analysis. A different approach to analyze diffraction by two incoherently superimposed gratings was investigated by Zhao et al. [17], [18]. They synthesized a volume-index grating vector and examined the Bragg matching and pseudo phase matching cases.

His theory was extended to consider multiple gratings recorded sequentially by one reference wave and object waves in a lossless holographic material and all waves in Bragg-matched condition [19]. We will derive equations that describe wave propagation in the same grating structure including off-Bragg matched condition and absorption gratings.

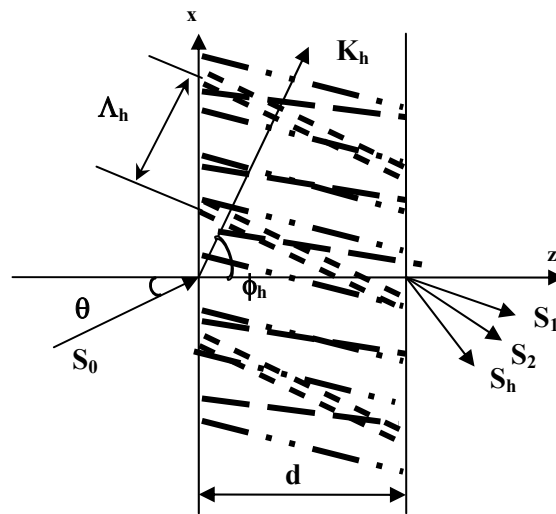


Fig. 1. Schematic illustration of the reconstruction of object waves illuminating on superimposed multiple gratings with a reference wave. S_0 : Reference wave amplitude, $S_{1\sim h}$: Signal wave amplitude, Λ_h : Grating period, K_h : Grating vector, d : Thickness.

We consider incoherently superimposed multiple gratings which are used in the design of beam combiners, beams splitters and beam couplers. Fig. 1 shows the basic model used in this analysis. We assume that the gratings are recorded in an optical material, which is infinite in the x and y direction, and all waves are propagating in the

x-z plane, and polarized in the y direction. The grating is defined by the grating vector \mathbf{K}_h and its length is $K_h=2\pi/\Lambda_h$, where Λ_h is the period of the h_{th} grating.

When the wave is polarized perpendicular to the plane of incidence, wave propagation in multiple gratings can be described by the scalar wave equation as

$$\nabla^2 E(x, z) + k^2 E(x, z) = 0 \quad (1)$$

where $E(x, z)$ is assumed to be independent of y and has an angular frequency ω . Material modulations constituting hologram gratings can be expressed by spatial variations of the relative dielectric constant ε and/or the conductivity σ . If ε_h and σ_h are the amplitudes of the spatial modulations of the h_{th} grating, the modulated quantities of ε and σ can be written

$$\begin{aligned} \varepsilon &= \varepsilon_0 + \sum_{h=1}^N \varepsilon_h \cos(\mathbf{K}_h \cdot \mathbf{X}) \\ \sigma &= \sigma_0 + \sum_{h=1}^N \sigma_h \cos(\mathbf{K}_h \cdot \mathbf{X}) \end{aligned} \quad (2)$$

where ε_0 is the average dielectric constant, σ_0 the average conductivity and $\mathbf{X}=(x, y, z)$.

We have the spatially modulated propagation constant k

$$k^2 = \frac{\omega^2}{c^2} \varepsilon - j\omega\mu\sigma \quad (3)$$

where c is the light velocity in free space and μ is the permeability of a material.

Inserting Eqn.(2) into Eqn.(3), we obtain

$$k^2 = \beta^2 - 2j\alpha\beta + \sum_{h=1}^N 2\beta\kappa_h (e^{-j\mathbf{K}_h \cdot \mathbf{X}} + e^{-j\mathbf{K}_h \cdot \mathbf{X}}) \quad (4)$$

where
$$\beta = \frac{\omega}{c} \sqrt{\epsilon_0} \quad , \quad \alpha = \frac{\mu c \sigma_0}{2\sqrt{\epsilon_0}} \quad (5)$$

and the coupling constant κ_h between the reference wave S_0 and the diffracted wave S_h by the h_{th} grating is

$$\kappa_h = \frac{\pi n_h}{\lambda} - j \frac{\alpha_h}{2} \quad n_h = \frac{\epsilon_h}{2\sqrt{\epsilon_0}} \quad \alpha_h = \frac{c\mu\sigma_h}{2\sqrt{\epsilon_0}} \quad (6)$$

where n_h and α_h are the spatial modulation amplitudes of the refractive index and the absorption constant respectively. Each diffracted wave and the reference wave have the propagation vectors ρ_h and ρ_0 respectively. We can obtain the following momentum equation:

$$\rho_h = \rho_0 - \mathbf{K}_h \quad (7)$$

We can construct the Bragg diagram in which all waves obey the Bragg condition as shown Fig.2 :

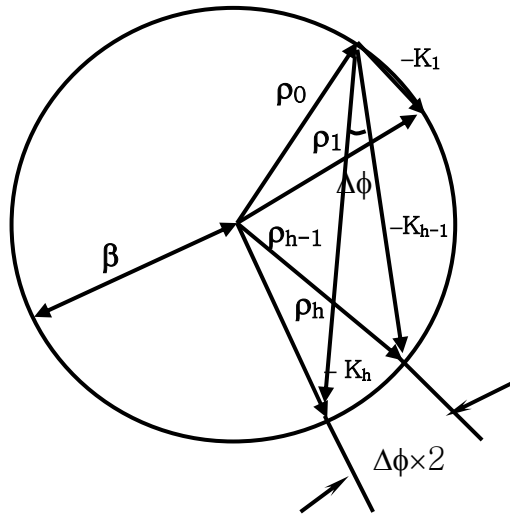


Fig. 2. Bragg matched diagram for multiple gratings.

From Fig. 2, it is clear that the angle difference between the h_{th} and the $h-1_{th}$ diffracted beam is twice that between the h_{th} and the $h-1_{th}$ grating. The components of ρ_0 and \mathbf{K}_h are given by

$$\rho_0 = \beta \begin{bmatrix} \sin \theta \\ 0 \\ \cos \theta \end{bmatrix}, \quad \mathbf{K}_h = K_h \begin{bmatrix} \sin \phi_h \\ 0 \\ \cos \phi_h \end{bmatrix} \quad (8)$$

At the Bragg angle, $\theta_{h_{Bragg}}$ of the h_{th} grating

$$\beta^2 - \rho_h^2 = 0 \quad (9)$$

We combine Eqn. (7) and (8), and insert into Eqn. (9) to obtain

$$\cos(\phi_h - \theta_{h_{Bragg}}) = K_h / 2\beta \quad (10)$$

Also, Eqn. (10) can be derived easily from the Bragg's law. Fig. 3 shows angle relationships between in grating layers and x-z plane.

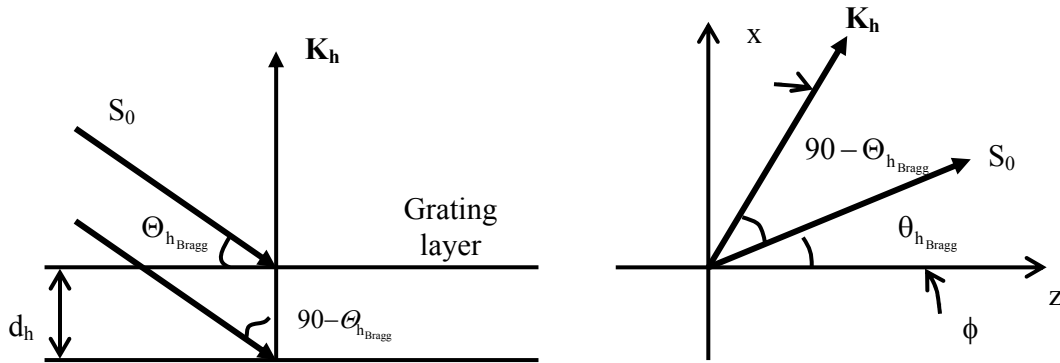


Fig. 3. Angle relationships between in grating layers and x-z plane.

The equations resulting from Bragg's law and angle relationships are

$$d_h = \frac{\lambda}{2 \sin \Theta_{h\text{Bragg}}} \quad (11)$$

$$\Theta_{h\text{Bragg}} = 90 - \phi_h + \theta_{h\text{Bragg}} \quad (12)$$

The grating period Λ_h is equal to d_h , and by inserting Eqn. (12) into (11) we can derive Eqn. (10).

We describe the waves in the medium of Fig.1 with complex amplitudes S_0 and S_h , which vary along z . The total electric field in the gratings can be written as:

$$E = S_0(z) e^{-j\rho_0 \cdot \mathbf{x}} + \sum_{h=1}^N S_h(z) e^{-j\rho_h \cdot \mathbf{x}} \quad (13)$$

By inserting Eqn. (4), (13) into (1), we obtain

$$\begin{aligned} & \left(S_0'' - 2jS_0' \rho_{0z} + (\beta^2 - \rho_0^2) S_0 - 2j\alpha\beta S_0 + 2\beta \sum_{h=1}^N \kappa_h S_h \right) e^{-j\rho_0 \cdot \mathbf{x}} \\ & + \sum_{h=1}^N \left((S_h'' - 2jS_h' \rho_{0z} + (\beta^2 - \rho_h^2) S_h - 2j\alpha\beta S_h + 2\beta \kappa_h S_0) e^{-j\rho_h \cdot \mathbf{x}} \right) = 0 \end{aligned} \quad (14)$$

where the primes indicate differentiation in the z direction.

The propagation vector of the reference wave S_0 , ρ_0 is equal to the wave propagation vector in the absence of the gratings. Hence, $\beta^2 - \rho_0^2$ becomes zero. We assume that the energy interchange between the diffracted orders is slow. Therefore, the second differential term can be neglected. The coefficient of each exponential must vanish individually. Defining the obliquity factors C_0 , C_h and dephasing measure \mathcal{G}_h for the h_{th} grating [1]:

$$C_0 = \frac{\rho_{0z}}{\beta} \quad C_h = \frac{\rho_{hz}}{\beta} \quad \mathcal{G}_h = \frac{\beta^2 - \rho_h^2}{2\beta} \quad (15)$$

Then, by the substitutions of Eqn. (15) for variables in Eqn. (14) and, the conditions on the energy exchange and reference wave propagation vector, we can obtain the differential equations Eqn. (16) which are generalized coupled wave equations for N superimposed gratings.

$$\begin{aligned} C_0 S_0' + \alpha S_0 &= -j \sum_{h=1}^N \kappa_h S_h \\ C_h S_h' + (\alpha + j\vartheta_h) S_h &= -j \kappa_h S_0 \end{aligned} \quad (16)$$

B. Simulation Results for Multiple Thick Holographic Gratings in Three Different Modes

The common-Bragg-angle structure with incoherently superimposed N gratings can be fabricated when holograms are recorded sequentially by one reference wave and N objective waves [15], [19]. The reference wave illuminates at the same incident angle during every exposure, and the incident angle of the object wave is changed at every exposure. It is noted that the reference wave is common to every exposure so that the N gratings have a common Bragg angle, when the readout wave has the same wavelength as that used for recording ($\theta_{1_{Bragg}} = \theta_{2_{Bragg}} = \dots = \theta_{N_{Bragg}} = \theta_{Bragg}$, The geometric description of $\theta_{h_{Bragg}}$ is shown in Fig. 3.). There are three different modes in which the common-Bragg-angle structure can be read out [15]. The first, called the beam-splitter mode, illuminates the structure with the reference wave at the common Bragg angle. The one input wave reconstructs N object waves. The second, called the beam-combiner mode, is the time-reversal case of the first one. For the beam-combiner mode, N object

waves illuminate the structure at each Bragg angle and reconstruct the reference wave. The third, called the cross-coupled mode, illuminates the structure with one of the object waves. For the cross-coupled mode, the input wave produces a diffracted wave in the direction of the reference wave. And then the reconstructed reference wave can diffract again into the directions of other object waves before leaving the grating structure.

We investigated efficiencies of the output waves for the cases of three different modes. It is assumed that a holographic material has six lossless dielectric gratings ($\alpha=0$) and all waves are in phase and the Bragg-matched condition ($\mathcal{G}_h=0$) is satisfied. By the assumption, Eqn. (16) can be written as

$$\begin{aligned} C_0 S'_0 &= -j \sum_{h=1}^6 \kappa_h S_h \\ C_h S'_h &= -j \kappa_h S_0 \end{aligned} \quad (17)$$

The efficiency of the output wave S_h is defined as [1]

$$\eta_h = \frac{|C_h|}{C_0} S_h S_h^* \quad (18)$$

Results from the combination Eqn. (7) and Eqn. (8) give the z component of the propagation vector of the object wave for the h_{th} grating. Inserting the results into Eqn. (15), the oblique factors C_0 and C_h , and the dephasing measure \mathcal{G}_h for the common Bragg angle structure in the Bragg matched condition can be written as:

$$C_0 = \frac{\cos \theta_{\text{Bragg}}}{\beta} \quad C_h = \cos \theta_{\text{Bragg}} - \frac{K_h \cos \phi_h}{\beta} \quad \mathcal{G}_h = 0 \quad (19)$$

where θ_{Bragg} is the common-Bragg-angle which is identical to the incident angle of the reference wave.

A grating strength for a single hologram was defined by Kogelnik [5] as

$$\nu = \frac{\pi n_1 d}{\lambda \sqrt{C_R C_O}} \quad (20)$$

where d is the thickness of a material, C_R and C_O are the obliquity factors of reference and object wave respectively, and λ is wavelength. We redefined the grating strength ν_h

for the h_{th} grating as :

$$\nu_h = \frac{\pi n_h d}{\lambda \sqrt{C_R C_h}} \quad (21)$$

We assumed that the grating strengths for the six gratings are equalized ($\nu_1 = \nu_2 = \nu_3 = \nu_4 = \nu_5 = \nu_6 = \nu$). The efficiencies of the waves at $z=d$ for three different boundary conditions such as beam combiner, splitter and cross-coupler modes are plotted as a function of the equalized grating strength normalized by $\nu_0 = \pi/2$ in Fig. 4, 5, 6, and 7. During hologram recording, beam S_0 is used for a reference wave and the others are objective waves. The common-Bragg-angle is $\pi/6$ and the first grating formed by the interference of beam S_0 and S_1 is non-slanted ($\phi_1 = \pi/2$). The order of gratings corresponds to that of the sequential interference of from beam S_1 to S_6 with reference wave S_0 . The incident angle difference between two object waves S_h and S_{h+1} is constant. For the splitter mode, the boundary conditions at $z=0$ are

$$S_1(0) = S_2(0) = S_3(0) = S_4(0) = S_5(0) = S_6(0) = 0, S_0(0) = 1 \quad (22)$$

where $S_0(z)$ is the amplitude of the reference wave and $S_1(z) \sim S_6(z)$ are the amplitudes of the six object waves. The 1:6 beam splitter divides the incident wave S_0 into the six waves which show equalized maximum diffraction efficiencies when the equalized

grating strength v is $0.204\pi \cong \frac{1}{\sqrt{6}} \frac{\pi}{2}$ as shown Fig. 4. A beam splitter with N superimposed gratings divides an incident wave into N partial waves which have equalized maximum diffraction efficiencies when the N grating strengths satisfy the equation, $\left(\sum_{h=1}^N v_h^2\right)^{\frac{1}{2}} = \frac{\pi}{2}$ [15], [19], [20]. It provides proof that the output waves of the 1:6 beam splitter from S_1 to S_6 reach maximum diffraction efficiencies when all grating strengths are equalized to $\frac{1}{\sqrt{6}} \frac{\pi}{2}$.

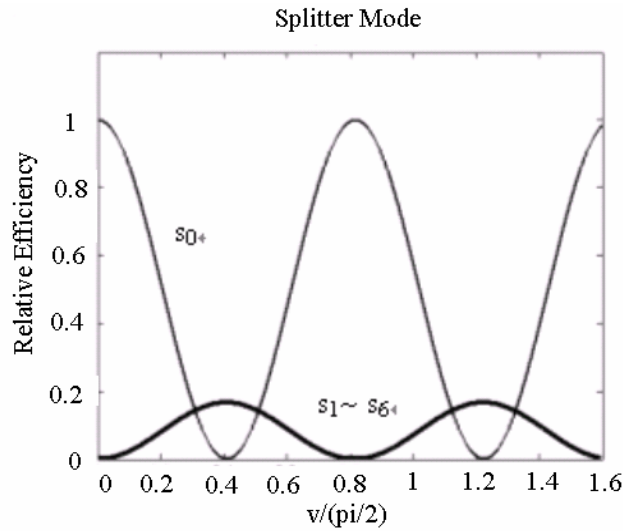


Fig. 4. Relative efficiencies η/η_0 for the splitter mode as a function of equal grating strengths normalized by $v_0=\pi/2$, the grating strength which gives a single hologram 100% diffraction efficiency. Peak efficiency of $\eta_0=1$.

For the combiner mode

$$S_1(0)=S_2(0)=S_3(0)=S_4(0)=S_5(0)=S_6(0)=1, S_0(0)=0 \quad (23)$$

By a time-reversal argument, a beam combiner must show maximum efficiency at the same grating strength as when a beam splitter reaches maximum diffraction efficiency.

Fig. 5 shows all input waves from S_1 to S_6 are fully combining and the output wave S_0

shows maximum efficiency at the grating strength as $\frac{1}{\sqrt{6}} \frac{\pi}{2}$.

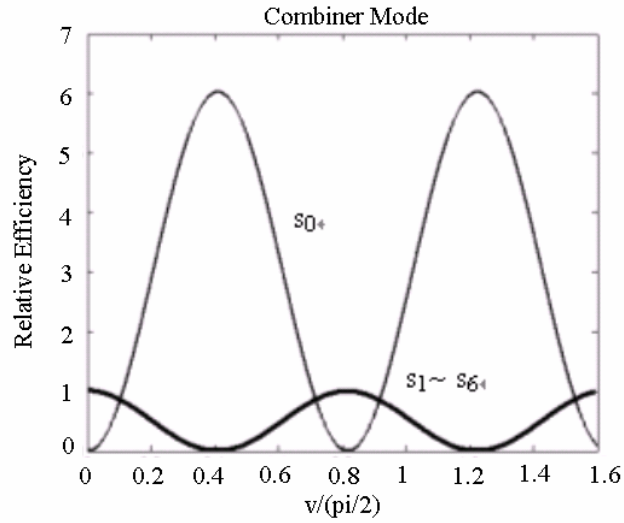


Fig. 5. Relative efficiencies η/η_0 for the combiner mode are plotted. All input beams are in phase. Peak efficiency of $\eta_0=1$.

For the cross-coupled mode, we consider two cases. In the first case, when an input wave is incoming along the direction of beam S_3 , the efficiencies of outgoing waves are analyzed. And the boundary conditions are

$$S_0(0)=S_1(0)=S_2(0)=S_4(0)=S_5(0)=S_6(0)=0, S_3(0)=1 \quad (24)$$

We note from Fig. 6 that at the grating strength 0.4π , the input wave is diffracted into the direction of beam S_0 and the reconstructed wave in the direction of beam S_0 is fully diffracted into the five object waves S_1, S_2, S_4, S_5, S_6 . The outgoing wave in the direction

of beam S_0 disappear and the efficiencies show equalized maximum values in the directions of the five object waves. However, at the grating strength 0.2π , the reconstructed wave in the direction of beam S_0 can not be diffracted again into the five object waves before leaving a holographic material and the efficiency of the output wave in the direction of beam S_0 reaches maximum.

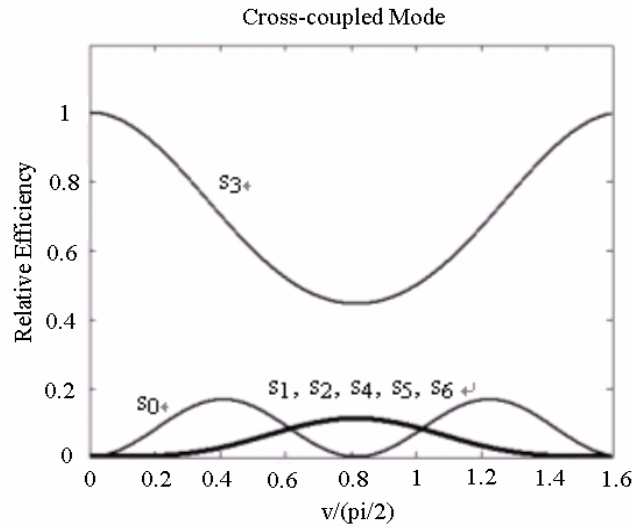


Fig. 6. Relative efficiencies η/η_0 for the cross-coupled mode are plotted. One input wave in the direction of beam S_3 is illuminating the 6 gratings. Peak efficiency of $\eta_0 = 1$.

In the second case, we consider the reversed case of the first. The five input waves are incoming along the directions of the five object waves S_1, S_2, S_4, S_5, S_6 and the efficiencies of outgoing waves are analyzed. The boundary conditions are

$$S_0(0)=S_3(0)=0, S_1(0)=S_2(0)=S_4(0)=S_5(0)=S_6(0)=1 \quad (25)$$

The efficiencies of outgoing waves are shown in Fig. 7. At the grating strength 0.4π , five input waves produce a diffracted wave in the direction of beam S_0 and this diffracted

wave is completely diffracted again into the direction of beam S_3 before leaving a holographic material. The outgoing wave in the direction of beam S_0 disappears and the efficiency of the output wave in the direction of beam S_3 shows maximum value. At the grating strength 0.2π , the five input waves are diffracted into the direction of beam S_0 and the reconstructed beam S_0 is partially diffracted again into the direction of beam S_3 . However, the reconstructed beam is mostly outgoing, and efficiency of the outgoing wave in the direction of beam S_0 reaches maximum.

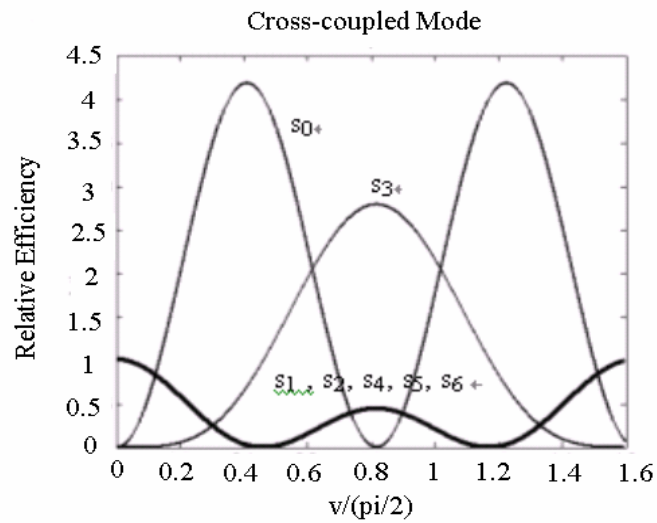


Fig. 7. Relative efficiency η/η_0 for the cross coupled mode are plotted. Five input waves, S_1, S_2, S_4, S_5, S_6 are illuminating the six gratings. Peak efficiency of $\eta_0 = 1$.

In experiment, it is difficult to perfectly equalize the intensities of all the input waves. Therefore, we investigate the influence of non-equal input beam intensities on the efficiency of beam combiner so that we may predict the sensitivity of the beam combiner for the real case. The efficiencies of the output waves for the case of non-equal amplitude inputs in the beam combiner mode are plotted in Fig. 8(a), (b) and (c). As shown, a smaller amplitude variation of the input intensities causes the smaller loss in output intensity compared to the sum of all the inputs. In Fig. 8(a), for the case that the amplitude difference between adjacent inputs is 16% of the strongest input amplitude, the output intensity of S_0 is about 76% of the sum of the intensities. Thus even in the worst case when the input amplitude difference is large, the output of S_0 shows only a 24% error. Figs. 8(b) and (c), show the output is 90% and 98% respectively when the amplitude difference is 10% and 5% respectively. Therefore, the output loss caused by non-equal input waves can be very small if the intensities of input waves are adjusted within 5%.

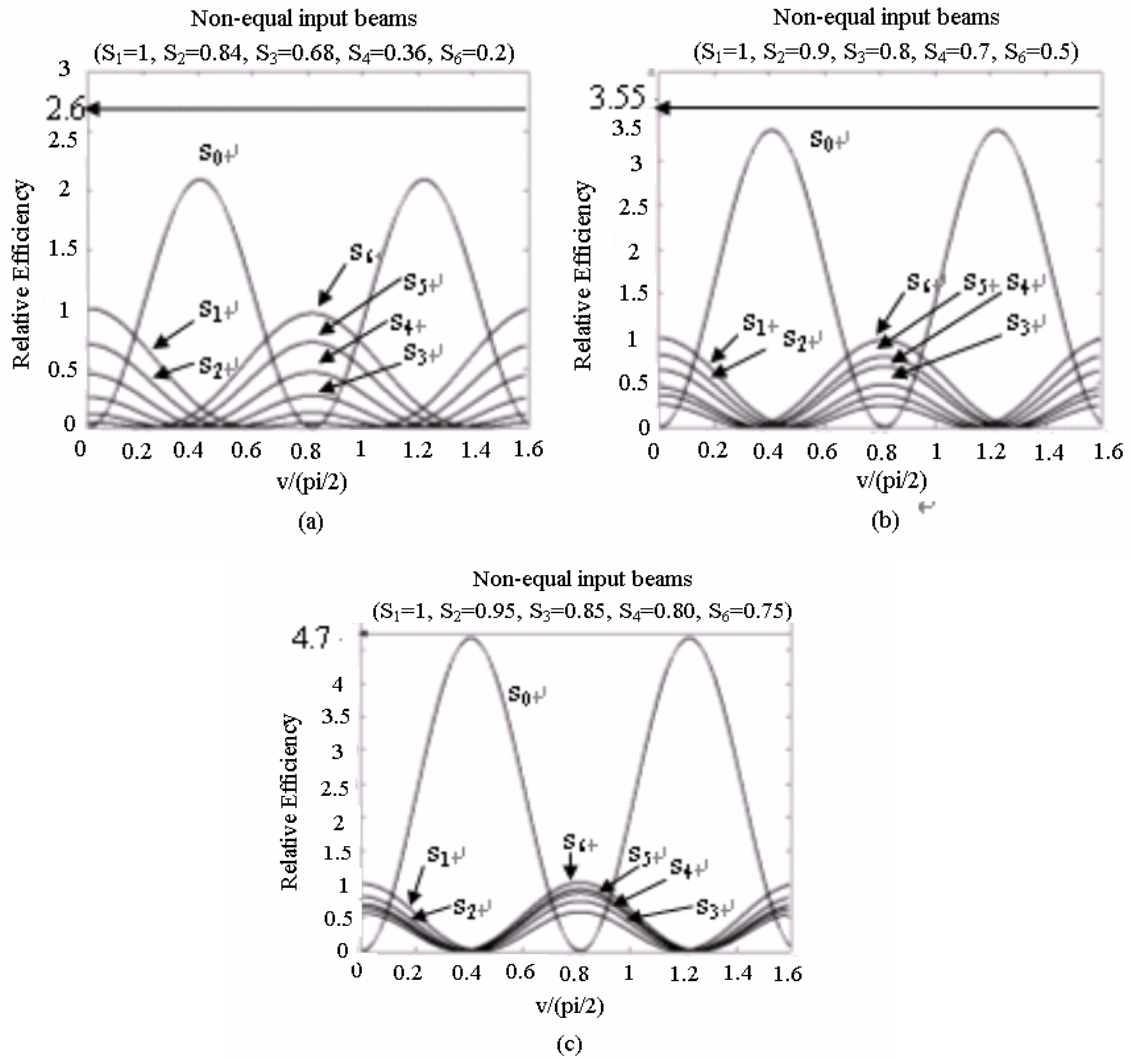


Fig. 8. Relative efficiency η/η_0 for six non-equal inputs in the beam combiner mode are plotted. Amplitude difference between adjacent two inputs set to three different values. (a) 0.16, (b) 0.1, (c) 0.05

III. CHARACTERIZATION OF THE RECORDING DYNAMICS OF A HOLOGRAPHIC MATERIAL AND RECORDING OF SIX HOLOGRAMS WITH EQUALIZED GRATING STRENGTHS

A. Introduction to Holographic material and Mechanism of Hologram Formation in a Photopolymer Material

Optical quality and thermal stability are important characteristics of holographic recording materials (HRMs). The dynamic range which determines the efficiencies and number of holograms recorded in the same spatial location, and signal to noise ratio are dependant on optical quality. During hologram recording and baking the dimensional change of HRMs is caused by thermal extension. Therefore, read-out should be performed at the compensated Bragg angle. Thermal stability minimizes the Bragg angle change. Therefore, thermal stability makes it simpler to read-out. In our experiment, a holographic material is selected because it has very good thermal stability and optical quality. The HRM used is a dye doped polymeric memplex [21]. The M/# of the material as claimed by the manufacturers is 9.42

A dye-doped polymer is composed of photosensitive monomeric dyes dispersed in a polymer host. Fig. 9 shows the mechanism of a hologram formation in a photopolymer [22]. Two coherent beams interfere within the photopolymer during holographic recording. The maximum light intensity of an optical interference pattern induces polymerization. But monomers do not react in a minimum intensity portion. Eventually, the initial spatial pattern of polymerization is generated by the optical

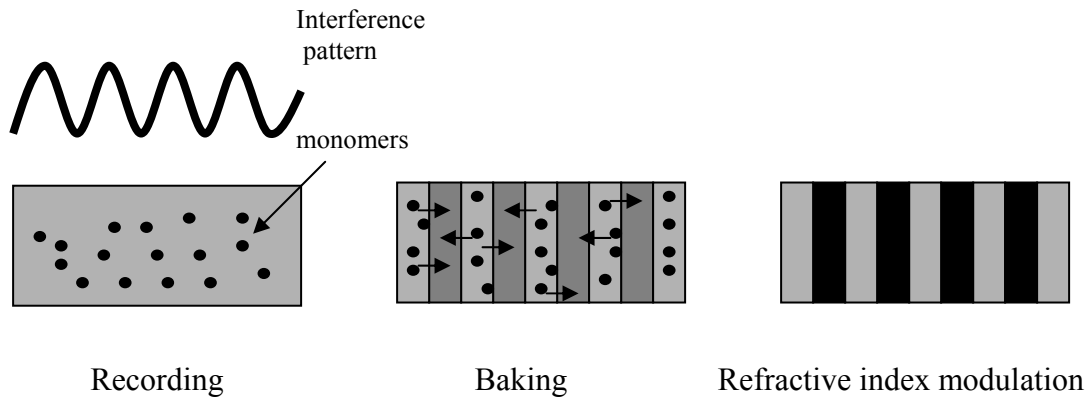


Fig. 9. Mechanism of hologram formation in a photopolymer system.

interference pattern, creating a concentration gradient. During the baking process, unpolymerized monomers diffuse into the initial polymerization portion and the concentration of the monomers in a material becomes uniform erasing the monomer grating, leaving only a polymer gratings determined by the difference between the refractive indices of the polymer host and polymerized dyes.

B. Demonstration of a Simple Technique for Determining the M/# of a Holographic Substrate Using a Single Exposure

We propose and demonstrate a potentially simpler technique to determine the M/# parameter for a holographic recording material. In this method, collimated object and reference beams are used to produce a spatially varying index modulation. The resulting diffraction pattern can be analyzed to find the M/# using only a single grating, to be contrasted with existing techniques that require many gratings.

The dynamic range of a holographic medium is an important parameter in determining the storage density and diffraction efficiency for holographic memory systems and holographic beam combiners [9], [10], [11], [12]. In these applications, many holographic gratings are multiplexed in the medium at the same spatial location. The $M/\#$ is a parameter that defines the dynamic range of the holographic medium; it is essentially $\pi/2$ times the ratio of the maximum achievable index modulation and the index modulation corresponding to a unity diffraction efficiency grating. The existing techniques [8], [9], [13], [14] to measure $M/\#$ require one to write many holograms in the material. In this section, we discuss a potentially simpler technique to determine the $M/\#$ for a holographic recording material and we present simulated and experimental results for a photopolymer-based holographic recording medium.

Typically, illumination of a holographic substrate with a spatially periodic, sinusoidal intensity pattern produces a periodic index modulation

$$n(x) \equiv n_o + n' \cos(K x) \quad (26)$$

where n_o is the spatially averaged index of refraction of the medium, n' is the index modulation depth, and K represents the wave number of the grating. When a laser beam of wavelength λ illuminates this grating at the Bragg angle, the diffraction efficiency η is given by [1]

$$\eta = \frac{I_d}{I_o} = \sin^2 \left(\frac{\pi n' \alpha d}{\lambda} \right) \quad (27a)$$

where I_o is the input intensity, I_d is the diffracted intensity and α is the obliquity factor determined by the orientation of the grating. For the case that a reference wave is

propagating in a x-z plane and material with a single grating is infinite in a x and y direction, α can be expressed as [1]

$$\alpha = \frac{I}{\sqrt{C_0 C_d}} ; C_0 = \frac{\rho_{0z}}{p}, C_d = \frac{\rho_{dz}}{p} \quad (27b)$$

where ρ_{0z} is the z-axis component of the propagation vector of the reference wave, ρ_{dz} is the z-axis component of the propagation vector of a diffracted wave and p is an average propagation constant in a material. A characteristic scale for the index modulation is $n_c \equiv \lambda / (2\alpha d)$, so that η becomes

$$\eta = \sin^2 \left(\frac{\pi n'}{2 n_c} \right); \quad \eta = 1 \quad \text{for} \quad n' = n_c \quad (28)$$

In many situations the modulation depth [5] can be modeled as

$$n' = n_m \left[1 - \exp \left(-\frac{t}{\bar{\tau}} \right) \right] \quad (29a)$$

where t is the exposure time, $\bar{\tau}$ is a time constant that depends on the material sensitivity and the intensity of the writing laser beams, and n_m is the maximum index modulation. A convenient way to quantify the value of n_m is through the use of the $M/\#$, which is defined as

$$M/\# = \frac{\pi n_m}{2 n_c} \quad (29b)$$

For notational convenience, we define a scaled version of this expression

$$Q \equiv \frac{n_m}{n_c}; \quad \text{so that} \quad M/\# = \left(\frac{\pi}{2} \right) Q \quad (29c)$$

When Q is an integer, it represents essentially the maximum number of orthogonal, unit

diffraction efficiency gratings that can ideally be written in a given spatial location.

Consider a situation where N equalized diffraction efficiency gratings are multiplexed on a single substrate using the Bragg (angle or wavelength) orthogonality condition. For $N \gg Q$ the diffraction efficiency for each grating can be approximated by $\eta \cong \left(\frac{\pi^2}{4}\right)\left(\frac{Q}{N}\right)^2$ [8], [9]. More generally, if the diffraction efficiencies of the gratings are not identical, it is possible to define and measure the M/# of the material [9] from the relation [8], [9]

$$Q \approx \sum_{i=1}^N \sqrt{\eta_i}, \quad \eta_i \ll 1 \quad (30)$$

To measure the M/# using this approach requires one to write many holograms. As an alternative method, one can also use the fact that the diffraction efficiency of a single grating in the small index modulation limit is a quadratic function (to the first order) of the exposure time, described by

$$\eta(t) \approx Q^2 \left(\frac{t^2}{\tilde{\tau}^2}\right) \left(\frac{\pi^2}{4}\right) \quad (31)$$

which follows directly from Eqns. (28), (29a), and (29c). The M/# can thus be determined from the curve that defines the diffraction efficiency of a single hologram as a function of exposure time. This method also requires recording many successive holograms with different exposures on the holographic substrate [9].

In this section, we offer a potentially simpler approach to determine the M/# from a single recording on the holographic medium. To illustrate this method, we first combine Eqns. (28) and (29a) to express the diffraction efficiency as a function of time:

$$\eta(t) = \sin^2 \left(\frac{\pi}{2} Q \left[1 - \exp \left(-\frac{t}{\tilde{\tau}} \right) \right] \right) \quad (32a)$$

Now, according to the generalized optical pumping model [9] the saturation rate ($\tilde{\tau}^{-1}$) depends linearly on the intensity of the radiation for writing the grating: $\tilde{\tau}^{-1} = \beta \tilde{I}$, where β is the sensitivity of the medium, and \tilde{I} is the amplitude of the intensity modulation defined as

$$I \equiv \tilde{I}(1 + \cos(K_G x)) \quad (32b)$$

with K_G being the grating vector. For typical values of \tilde{I} used, the value of β can be assumed to be a constant. If the value of \tilde{I} depends on position \vec{r} as well, then we can write

$$\eta(t, \vec{r}) = \sin^2 \left(\frac{\pi}{2} Q \left[1 - \exp(-\beta \tilde{I}(\vec{r}) t) \right] \right) \quad (33)$$

As a specific example, let us consider a situation when two equal intensity, coherent Gaussian beams write a grating in the holographic medium. The intensity distribution will be:

$$I(\vec{r}) = 2I_0 \exp\left(-\frac{2r^2}{\omega_0^2}\right) \left[1 + \text{Cos}(\vec{K}_G \cdot \vec{r}) \right]; \quad \vec{K}_G = \vec{K}_1 - \vec{K}_2 \quad (34)$$

where \vec{K}_1 and \vec{K}_2 are the propagation wave vectors, I_0 is the intensity at the center of each beam, and ω_0 is the Gaussian beam radius of each writing beam. Comparing Eqn.

(34) with Eqn. (32b), we find: $\tilde{I} = 2I_0 \exp\left(-\frac{2r^2}{\omega_0^2}\right)$. When this expression is used in Eqn.

(33), the resulting diffraction efficiency is given by

$$\eta(t, \bar{r}) = \sin^2 \left(\frac{\pi}{2} Q \left[1 - \exp \left(-f(r) \frac{t}{\tau} \right) \right] \right); \quad 0 \leq f(r) \leq 1 \quad (35)$$

where $f(r) = \exp \left(-\frac{2r^2}{\omega_0^2} \right)$, and $\tau = \frac{1}{2\beta I_0}$. Across the spatial profile of the writing beams, the value of $f(r)$ varies from 1 in the center for $r = 0$ to a value of 0 for $r \gg \omega_0$.

Now, if $\frac{t}{\tau} \approx 5$, for example, then at $r=0$, $\exp \left(-f(r) \frac{t}{\tau} \right)$ approaches zero. However, for $r \gg \omega_0$, so that, $f(r) \ll \frac{1}{5}$, $\exp \left(-f(r) \frac{t}{\tau} \right)$ approaches unity. This argument holds for larger value of $\frac{t}{\tau}$ as well. Therefore, for $\frac{t}{\tau} \geq 5$, the quantity $1 - \exp \left(-f(r) \frac{t}{\tau} \right)$ varies *monotonically* from 1 to zero. Therefore, the total number of circular fringes is always of the order of $Q/2$ for $\frac{t}{\tau} \geq 5$. To be more precise, let us express Q as follows:

$$Q = 2m + n + \alpha; \quad \alpha < 1, \quad n = 0 \text{ or } 1 \quad (36)$$

Consider first the case where $n=0$, and $\alpha=0$. In this case, for $\frac{t}{\tau} \geq 5$, the number of full circular fringes equals m with a null at the center. Consider next the situation where $n=1$, and $\alpha=0$. In this case, the number of full circular fringes will still be m , but there will be a peak at the center. Finally, for $\alpha \neq 0$, the efficiency at the center will have a dip if $n=1$, and a peak if $n=0$. The actual value of the efficiency at the center reveals the value of α .

We studied the phenomenon using simulations. Fig. 10(a) shows the result for exposure time dependence of the diffraction efficiency for an even Q value material with a plane wave read-out. Fig. 10(b) shows the case for an odd Q value material with a Gaussian beam read-out. The diffracted wave in this case shows the Gaussian envelope of the read-out beam. These results also confirm that the center of the diffraction pattern

appears dark for an even Q valued material and bright for an odd Q valued material. Fig. 11 shows the simulation result for diffraction for a material with a fractional Q value. The intensity at the center of diffraction pattern yields the value of α as 0.2, resulting in a Q value of 10.2 for Fig. 11(a), and 11.2 for Fig. 11(b) corresponding to the respective M/# values of 16.014, and 17.584.

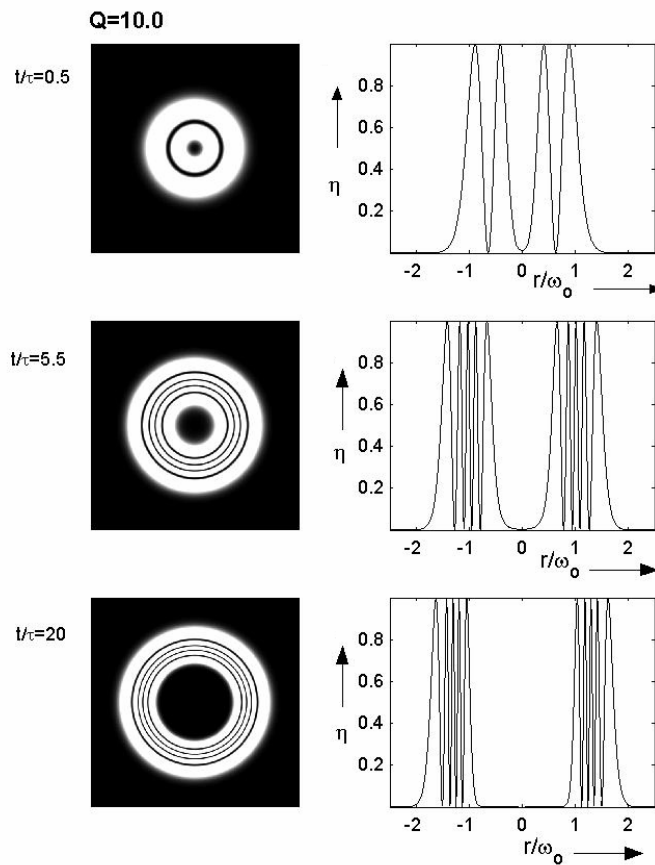


Fig. 10(a). Simulation results showing the evolution of diffracted pattern as a function of holographic exposure for an even Q ($m=5$, $n=0$, $\alpha=0$ in Eqn. (36)) value material with a plane wave read-out beam.

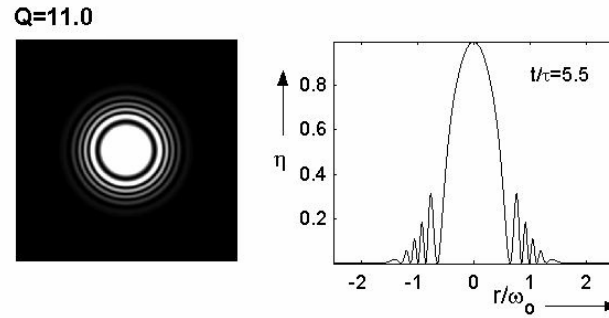


Fig. 10(b). Simulation result showing the diffracted pattern for an odd Q ($m=5$, $n=1$, $\alpha=0$ in Eqn. (36)) value material with a Gaussian read-out beam.

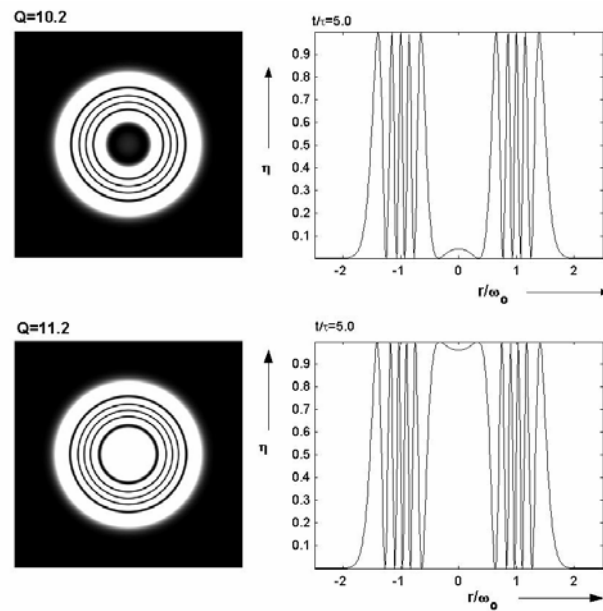


Fig. 11. Simulation results for the diffraction pattern for fractional Q with a plane wave read-out beam. (a). $m=5$, $n=0$, $\alpha=0.2$ in Eqn. (36); (b). $m=5$, $n=1$, $\alpha=0.2$ in Eqn. (36).

To show the principle of operation experimentally, we used a dye-doped polymeric Memplex[®] [21] material. This material had a Q value of 6 as claimed by the manufacturer. Fig. 12 shows the combined setup for hologram writing, and readout.

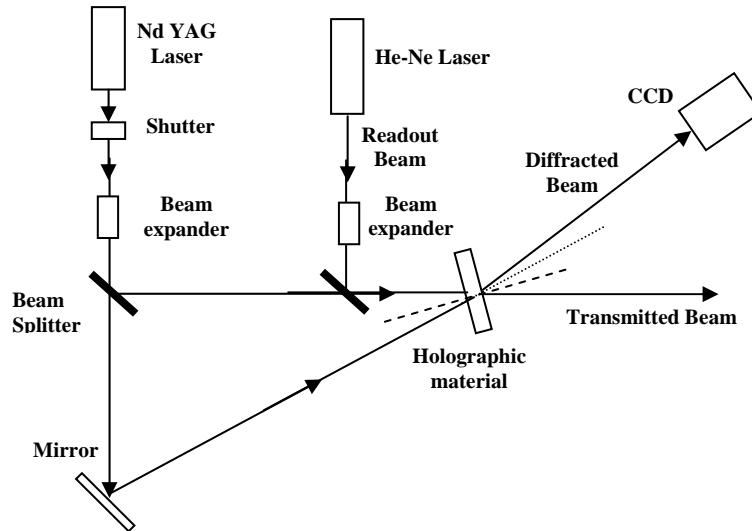
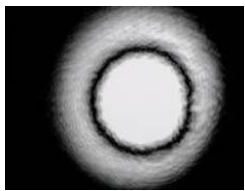
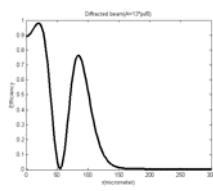
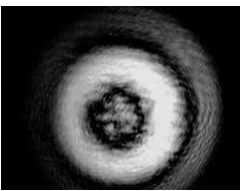
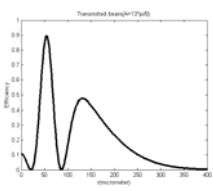
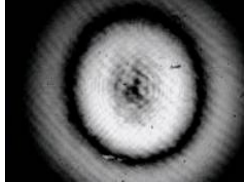
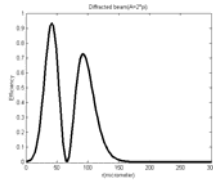
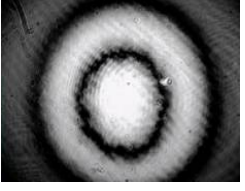
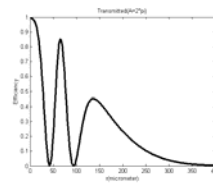

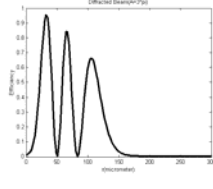

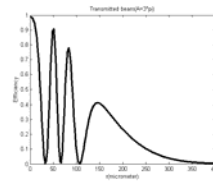


Fig. 12. Writing and Read-out Geometry.

Writing was done with a frequency doubled Nd:YAG laser ($\lambda=532$ nm) and readout was performed with a He-Ne laser operating at 632.8 nm. This material required baking after holographic exposure. During the experiment, the exposure times were gradually increased. After the exposure, the material was baked until the number of observable interference fringes reached maximum. Table 1 shows the results for a series of exposures for the holographic substrate. It shows that as we reach the optimum limit for holographic exposure, the number of interference fringes visible in the diffracted beam reach a maximum (3 in this case). Thus, the Q for our material is ~ 6 . This value of Q

yields the $M/\#$ of the material as 9.42.

Table 1. Experimentally observed transmission and diffraction patterns for 3 different exposures. As one reaches the optimum limit for holographic exposure, the number of interference fringes visible in the diffracted beam reach a maximum.

S.N.	Exp. Time (Sec)	Diffracted Image	Profile of the Diffracted Image	Transmitted Image	Profile of the Transmitted Image
1	26				
2	52				
3	120				

We have proposed and demonstrated a simple approach to determine the $M/\#$ parameter for any holographic recording material. This easy-to-use technique will be very attractive for holographic data storage where *a-priori* knowledge about the storage material is valuable in determining the storage density and recording schedule for the holograms.

C. Exposure Schedule and Holographic Recording Set-up Using Angular Multiplexing

Uniform diffraction efficiencies can be achieved by assigning an equal grating strength to each hologram [23], [24]. The maximum equal grating strength which can be assigned to one of six holograms is $\pi/2$, because our material has a saturation grating strength of 3π . Fig. 5 in Section II shows that the efficiencies of the output waves in the combiner mode are periodic functions of the equal grating strength. The input beams $S_1 \sim S_6$ are completely combined into the output beam S_0 at the equalized grating strength as $0.204\pi + 0.408\pi (\approx \frac{1}{\sqrt{6}}\pi)N$, where N is zero and a positive integer. It is determined that, to obtain the best diffraction efficiency within the available dynamic range of our material, the equal grating strength should be 0.204π at which a six-beam combiner reaches the first maximum diffraction efficiency.

The required exposure and baking time to achieve a grating strength of $\pi/2$ was measured by recoding a single hologram. The material was exposed for 8 seconds and baked for one and half hours. The equal grating strength desired for a six beam combiner is 0.204π . Therefore an exposure time for the 1st grating decreases less than 8s in order to obtain the grating strength 0.204π .

To record equal grating strength holograms using all available dynamic ranges of the recording media, exposure time for the sequence of holograms is determined as follows. If all holograms are recorded with a constant exposure, holograms recorded earlier in a superposition can be partially erased by a later exposure. Therefore this decay results in non-uniform diffraction efficiency. To balance the diffraction efficiencies of all holograms, the exposure time decreases with order of holograms [25]. The exposure time

for the 1st hologram was 4s so that the grating strength could reach 0.204π . The exposure times from the 2nd to 6th decreased gradually as the order of holograms increased. Table 3 in Section D shows an exposure time for each order of holograms.

Six holograms can be superimposed by in-plane angular multiplexing [26], [27] as shown in Fig. 13. The reference and object beams are plane waves. Each hologram can be addressed by changing the incident angle of each object wave. The reference and object waves are on the same plane. Fig. 14 shows a hologram recording set-up with plane waves using angular multiplexing. The laser beam from the light source is expanded and collimated, and is split into two beams. The incident angle of the reference wave is fixed and the rotation of two mirrors changes the incident angles of the object waves so that the hologram gratings have different Bragg angles, Θ_{Bragg} defined in Fig. 3. However, a common Bragg angle θ_{Bragg} can exist because the reference wave S_0 has the common incident angle during every exposure. The reference and object waves are interfered within a dye doped photopolymer.

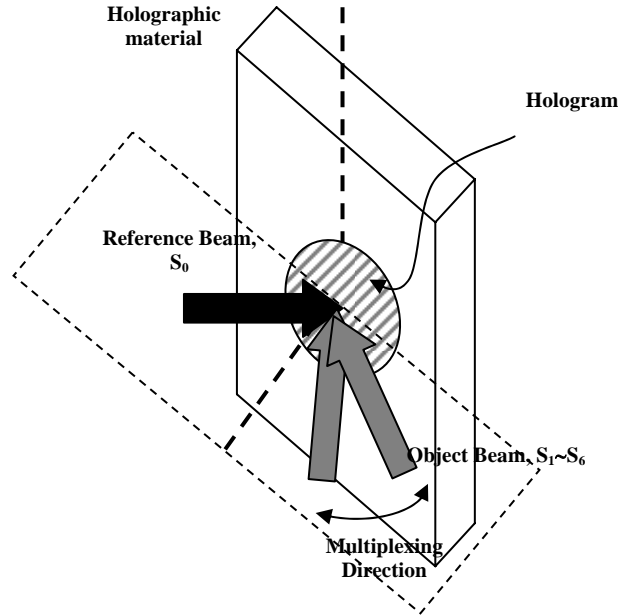


Fig. 13. Angle multiplexing, in-plane.

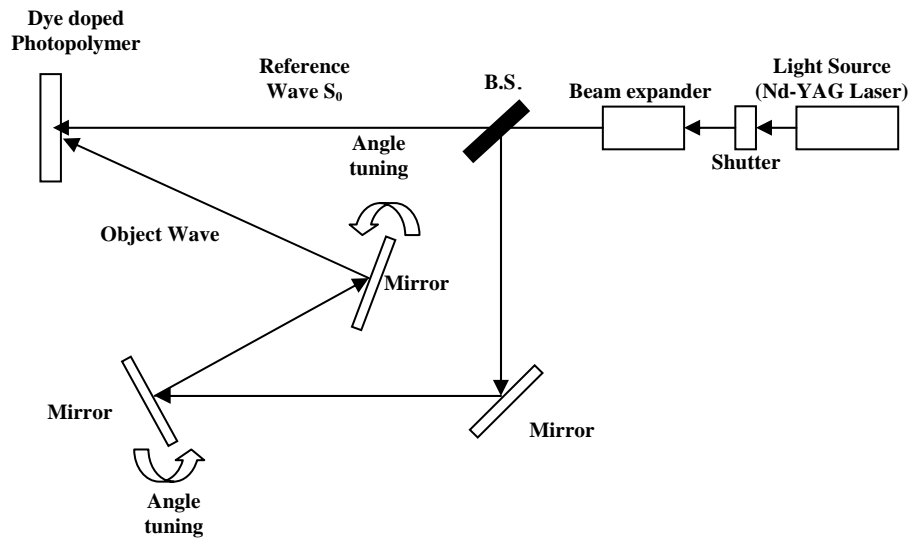


Fig. 14. Experimental set-up for holographic recording using angular multiplexing.

D. Determination of Equalized Grating Strength Analyzing Output Waves in the Beam

Splitter Mode

We estimate equalized grating strength of analyzing output waves when an input wave propagates along the direction of the reference wave. The input wave S_0 illuminates N superimposed holograms with equalized gratings at the common Bragg angle and is diffracted into waves $S_1 \sim S_N$. The output waves $S_1 \sim S_N$ propagate along the direction of each object wave. The coupled wave equations for refractive index modulated multiple superimposed gratings in a lossless material, and all waves in the Bragg matched condition can be derived from Eqn. (16) and written as [15], [20]

$$C_0 S_0' = -j \sum_{h=1}^N \kappa_h S_h, \quad C_h S_h' = -j \kappa_h S_0 \quad (37)$$

The boundary conditions for the waves at $z=0$ are

$$S_0(0)=1, S_1(0)= S_2(0)= \dots \dots = S_N(0)=0 \quad (38)$$

We are interested in the amplitudes of output waves at $z=d$. The solutions of the differential equations at $z=d$ are written as [15], [20]

$$S_0(d) = \cos\left(\sqrt{\sum_{h=1}^N \nu_h^2}\right), \quad S_k(d) = -j \frac{\nu_k}{\sqrt{\sum_{h=1}^N \nu_h^2}} \sin\left(\sqrt{\sum_{h=1}^N \nu_h^2}\right) \quad (39)$$

where ν_h is the grating strength for the h_{th} hologram

Holograms are recorded with a Gaussian beam and the index modulation amplitude is propositional to the intensity of a recording beam. The grating strengths of

all holograms are equalized and show the Gaussian profile along the beam radius.

Therefore, the grating strength for each hologram can be expressed as

$$v_h = \frac{\pi n_h d}{\lambda \sqrt{C_0 C_h}} = A \exp\left(-\frac{2r^2}{\omega_0^2}\right), \quad (h=1 \sim N, v_1 = v_2 = \dots = v_N = v) \quad (40)$$

where C_0 and C_h are the obliquity factors of S_0 and S_h respectively, n_h are the index modulation amplitudes, A is an equalized grating strength value at the center of the recording beam, ω_0 is the Gaussian beam radius of the recording beam, and λ is wavelength. Readout is performed at the same wavelength as that used for hologram recording. By the combination of Eqn. (39) and the Eqn. (40), S_0 and S_h can be written as

$$S_0(d) = \cos\left(\sqrt{N}A \exp\left(-\frac{2r^2}{\omega_0^2}\right)\right), \quad S_h(d) = -j \frac{1}{\sqrt{N}} \sin\left(\sqrt{N}A \exp\left(-\frac{2r^2}{\omega_0^2}\right)\right) \quad (41)$$

The readout beam also shows the Gaussian profiles in the r spatial domain. Multiplying Eqn. (41) by a Gaussian envelope, the amplitude behavior of outgoing waves at $z=d$ in r spatial domain can be expressed by

$$\begin{aligned} S_0(r) &= \cos\left(\sqrt{N}A \exp\left(-\frac{2r^2}{\omega_0^2}\right)\right) \exp\left(-\frac{r^2}{\omega_1^2}\right) \\ S_h(r) &= -j \frac{1}{\sqrt{N}} \sin\left(\sqrt{N}A \exp\left(-\frac{2r^2}{\omega_0^2}\right)\right) \exp\left(-\frac{r^2}{\omega_1^2}\right) \end{aligned} \quad (42)$$

where ω_1 is the Gaussian radius of the reading beam. From Eqn. (42), it is observed that when N superimposed holograms are considered as a single hologram, an effective accumulative grating strength for N holograms at the center of beam is \sqrt{N} times the equalized grating strength noted as A . We can insert Eqn. (42) into Eqn. (18) and finally arrive at the efficiency of the output wave as a function of r

$$\eta_h = \frac{|C_h|}{C_0} S_h(r) S_h^*(r) , (h=0 \sim N) \quad (43)$$

where $S_h^*(r)$ is the conjugate of $S_h(r)$.

We study the efficiencies of transmitted and diffracted beams for our case of six superimposed refractive index gratings recorded using angular multiplexing with the common Bragg angle. As shown Fig. 4, the diffraction efficiencies of the output waves periodically oscillate as the equalized grating strength increases. We calculated the relative diffraction efficiencies for four different equalized grating strengths at which a beam splitter reaches the first, second maximum and minimum as shown Fig. 4. Fig. 15 shows the relative efficiencies as given by Eqn. (43) when the grating strength, A at the center of the beam is equal to the equalized grating strength of: $\nu = 0.204\pi$ at the first maximum efficiency, $\nu = 0.404\pi$ at the first minimum, $\nu = 0.612\pi$ at the second maximum, and $\nu = 0.812\pi$ at the second minimum as shown Fig. 4. The number of minimum points of the transmitted beam S_0 increases as the center-equalized grating strength increases. Fig. 16 shows efficiencies of the transmitted beams S_0 for a single hologram when a grating strength for a single hologram is equal to the effective accumulative grating strength as $\sqrt{N} \times A$. By the comparison of Fig. 15 with Fig. 16, we note that the number of rings in the transmitted beam for each case in Fig. 15 is equal to that for each single hologram which has the same grating strength as the effective accumulative grating strength of the superimposed holograms.

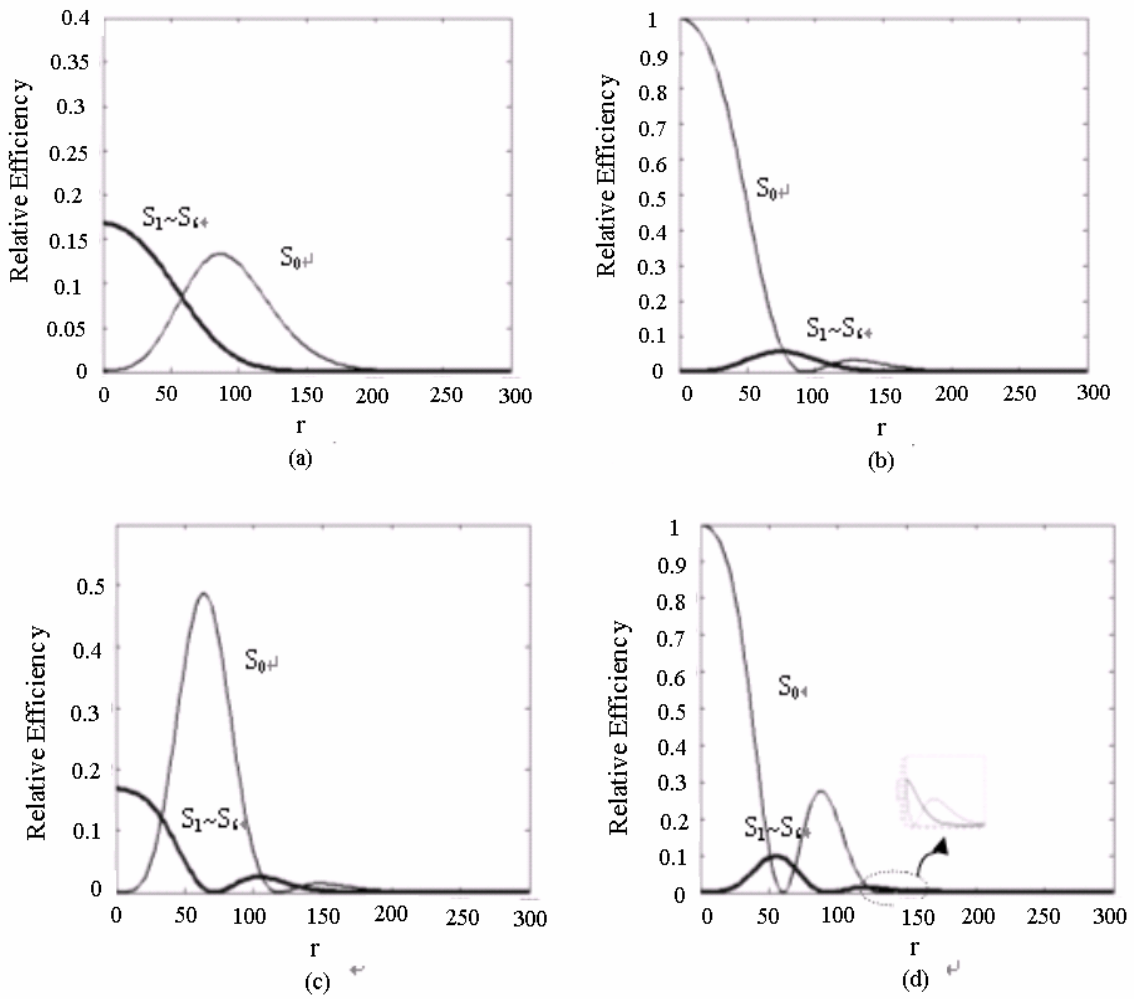


Fig. 15. Efficiencies of output beams as a function of beam radius for four different center-equalized grating strength with a Gaussian read-out beam. (a) $A = 0.204\pi$ (b) 0.404π (c) 0.612π (d) 0.812π (The unit of beam radius: μm , the portion inside the dashed circle is magnified in the small box, Peak efficiency of $\eta_0=1$, Relative efficiency = η/η_0).

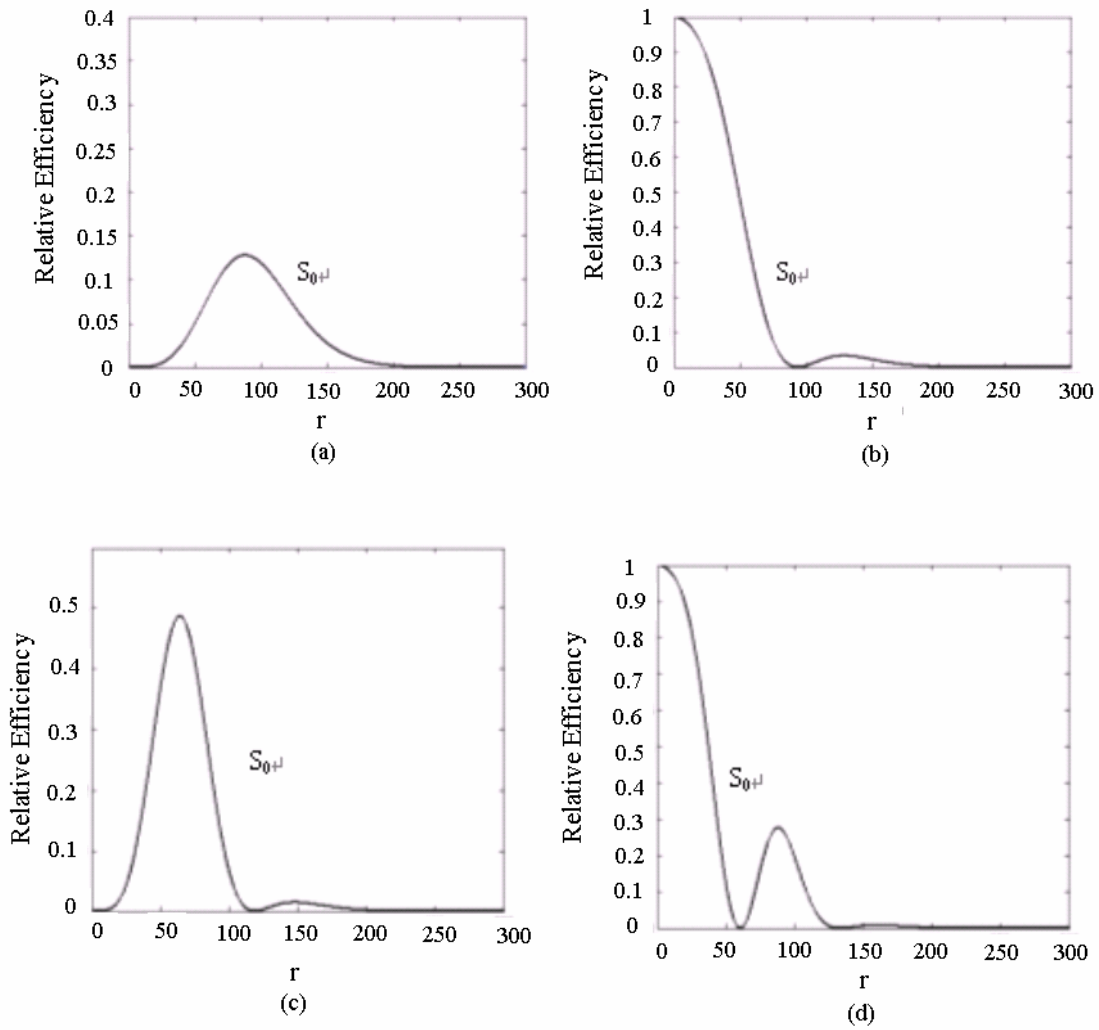


Fig. 16. Efficiencies of the transmitted beams of single holograms for four different grating strengths with a Gaussian read-out beam. (a) $0.204\pi \times \sqrt{6}$ (b) $0.404\pi \times \sqrt{6}$ (c) $0.612\pi \times \sqrt{6}$ (d) $0.812\pi \times \sqrt{6}$ (The unit of beam radius: μm , Peak efficiency of $\eta_0=1$, Relative efficiency = η/η_0).

Fig. 17 shows the combined setup for hologram writing and readout. The recording laser is a Nd-YAG laser ($\lambda=532\text{nm}$) and read-out is performed with the same laser. We recorded four holograms in one sample and six holograms in the other sample with different exposure schedule using angular multiplexing. In this set-up, the incident angle of the reference wave S_0 is fixed during every exposure. Therefore, a common Bragg angle can exist. In readout, a beam illuminate the holograms at the common Bragg angle and beams $S_1\sim S_N$ are reconstructed simultaneously in the Bragg matched condition. The holographic material with four holograms was baked for 3 hours and that with six holograms for 2 hours. We compared observed experimental images with simulation results from optional A values and evaluated the optimized A value which makes efficiency profiles identical to the experimentally observed images of output waves. Table 2&3 show the transmitted and diffracted images of four and six superimposed holograms, exposure schedules, and simulation results. In Table 2, the diffraction image of S_2 shows low efficiency as compared with that of S_1, S_3, S_4 and a fringe in the bright region inside the ring because of a mode hopping of the laser during the 2nd exposure. However, by the comparison of the number of rings observed in the images with the profiles, it is determined that the equalized grating strength of four holograms is 1.08π . From Table 3, it is determined that the equalized grating strength of the six holograms is 0.23π . It is higher than 0.204π which is the value at which a beam splitter shows the first maximum diffraction efficiency. Nevertheless, we can still expect the sample will function as a high efficiency beam splitter. Therefore, the sample will also function as a high efficiency beam combiner because of the time-reversal argument.

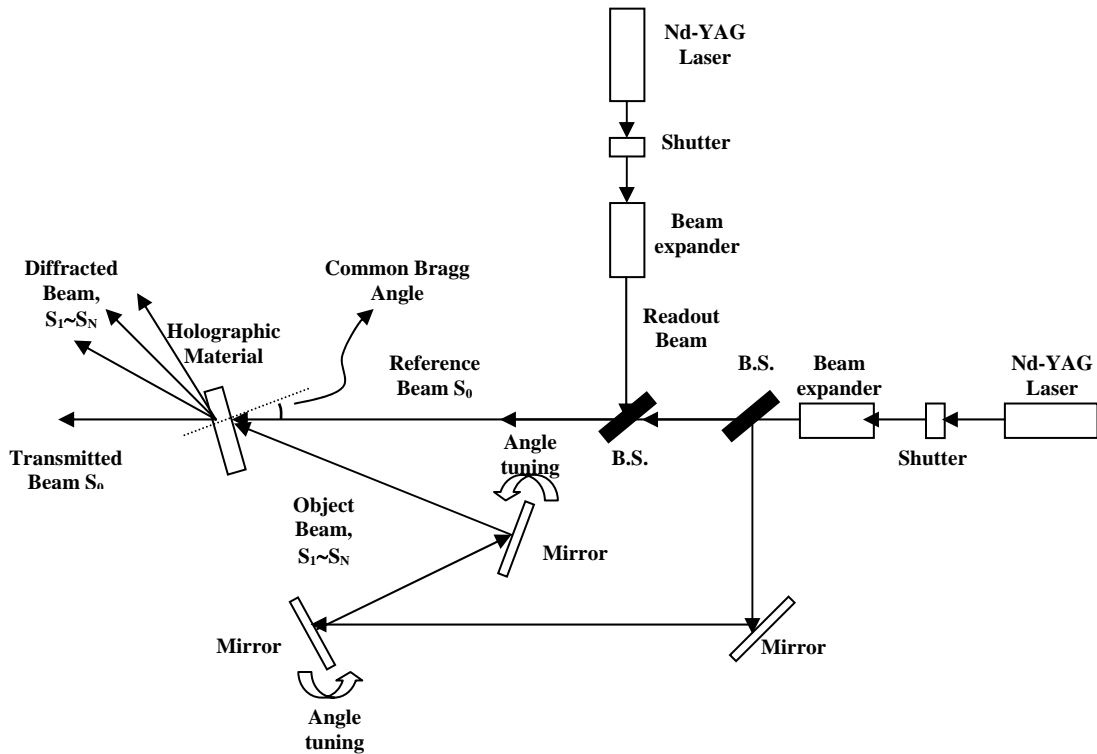


Fig. 17. Recording set-up with Nd-YAG laser using the angular multiplexing and read-out with the identical laser.

We demonstrated the technique to measure the equalized grating strength of N superimposed holograms with a common Bragg angle. It is very useful for determining the recording schedule to obtain the equalized grating strength desired for high efficiency multiple beam combiner and splitter.

Table 2. Experimentally observed transmission and diffraction patterns for 4 superimposed gratings. The profiles show the relative efficiency η/η_0 , as a function of beam radius. (The unit of beam radius: μm , Peak efficiency of $\eta_0=1$).

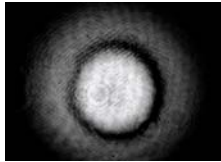
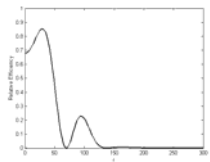
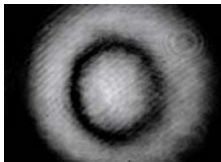
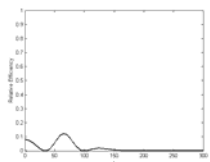

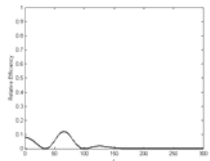
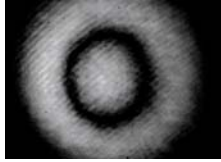
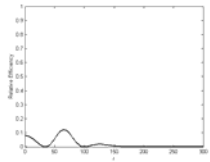
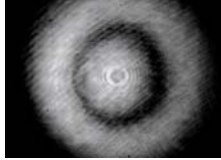
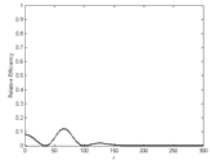
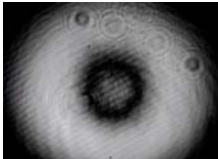
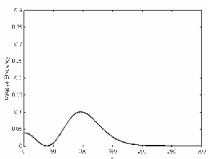
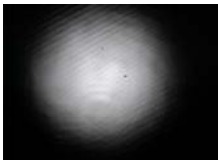
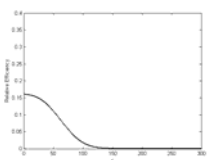
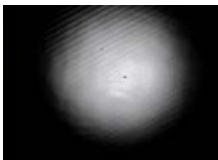
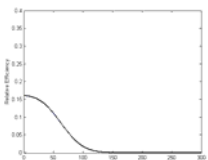

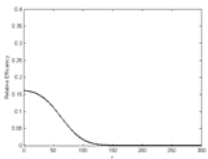
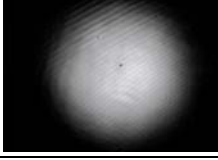
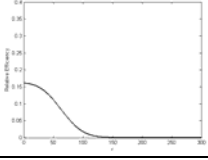

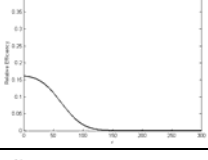
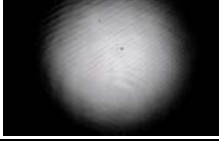
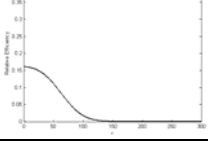
$A=1.08\pi$	Exposure Time (Sec)	Images	Profiles
S_0			
S_1	13		
S_2	13		
S_3	17		
S_4	21		

Table 3. Experimentally observed transmission and diffraction patterns for 6 superimposed gratings. . The profiles show the relative efficiency η/η_0 , as a function of beam radius. (The unit of beam radius: μm , Peak efficiency of $\eta_0=1$).

$A=0.23\pi$	Exposure Time (Sec)	Images	Profiles
S_0			
S_1	4		
S_2	3.5		
S_3	3.5		
S_4	3.2		
S_5	3.2		
S_6	3.2		

IV. BEAM COMBINATION USING SERVOS AND LOCK-IN AMPLIFIERS

A. Design of a Lock-in Amplifier Using an Analog Devices' AD630AD

A lock-in amplifier is composed of two main parts, a demodulator (mixer) and a low pass filter. The demodulator accepts two inputs. One is for a reference (carrier) and the other for a signal. The demodulator produces the product of the reference and the signal. Fig. 18 demonstrates how the lock-in amplifier detects the phase difference of noise-free two sinusoids which have the same frequency f . The signal phase is shifted by θ with respect to the reference. The demodulator output is a sinusoid whose frequency is twice the reference frequency and dc component is proportional to the cosine of the phase difference between the reference and signal. The lock-in amplifier output yields the dc component of the sinusoid signal by low-pass filtering.

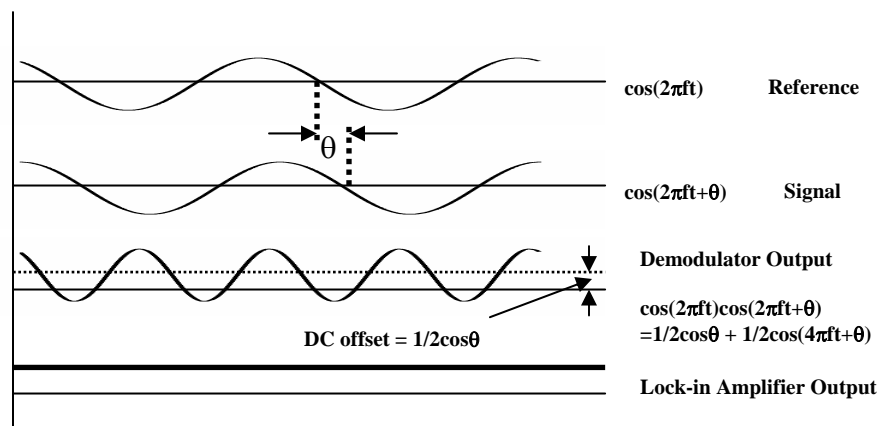


Fig. 18. Lock-in amplifier detects the phase difference between two sinusoids identified as “Reference” and “Signal”.

The lock-in amplifier was implemented using Analog Device's AD630AD as shown in Fig. 19. The AD630AD with electronic components operates by multiplying an applied modulated signal to the modulated input by a sinusoid at the same frequency as the carrier signal of the modulated signal [3]. The sinusoid applies to the carrier input. A low pass filter is fed into the demodulator output to remove AC components from the desired DC output. The output filter consists of two stages of the 6dB/octave roll-off low pass filter whose maximum gain and time constant are tunable by potentiometers.

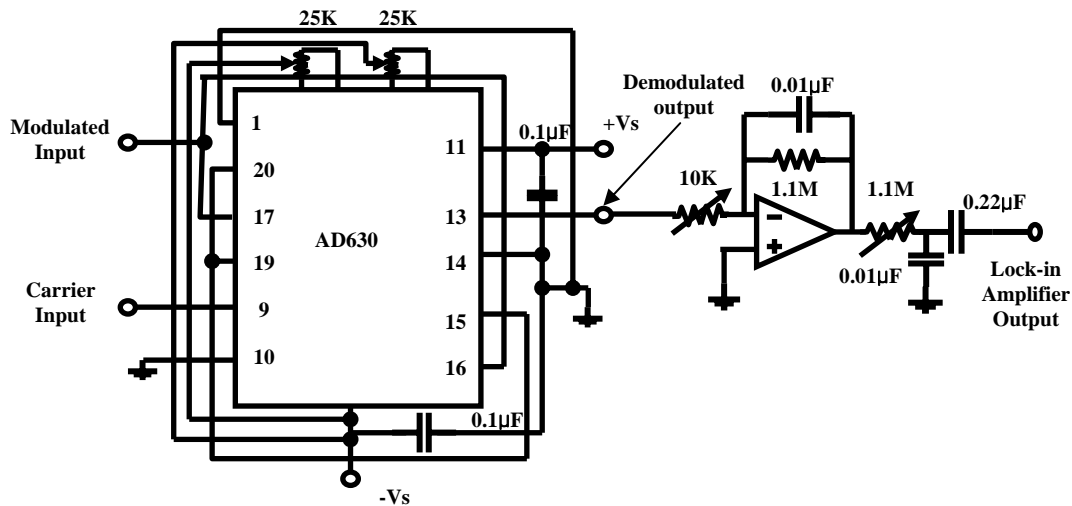


Fig. 19. AD630 with external electronic components functions as demodulator followed by two stage of low pass filter.

B. Beam Combination Using PZT Controller and Multiplexed Six Holograms

A Nd-YAG laser was used to record the six holograms by the interferences of one common reference wave, S_0 and six object waves, $S_1 \sim S_6$. A beam from the Nd-YAG laser is expanded three times while maintaining collimation, and then split into six

beams using beam splitters and mirrors as shown Fig. 20. The six beams illuminated the six superimposed gratings in the direction of the six object waves and were diffracted into the direction of the reference wave.

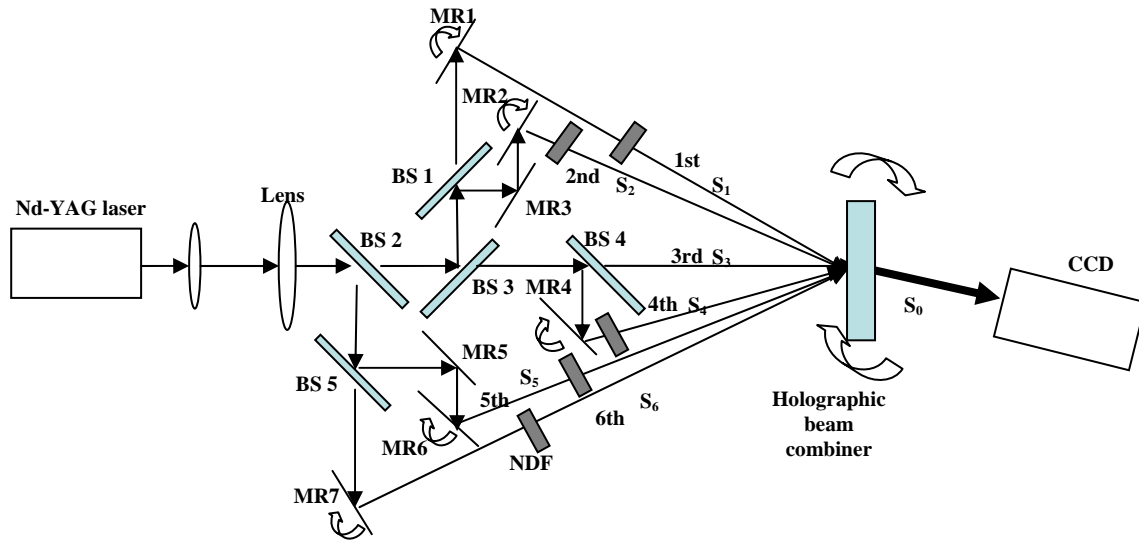


Fig. 20. Experimental set-up for beam combining. BS: beam splitter, MR: mirror, NDF: neutral density filter.

Each input wave was positioned at the Bragg angle of each grating by using the following procedure. A holographic beam combiner was mounted on a rotation stage. The rotation of the beam combiner caused the fixed 3rd beam to position at the Bragg matched angle for the 3rd grating. The rotation stage was fixed at the Bragg angle of the 3rd grating. Then the 1st beam was positioned at the Bragg angle for the 1st grating adjusting B.S. 3 and M.R. 1. After setting B.S. 3 and M.R. 1 and positioning the 1st beam, the 2nd beam was positioned at the Bragg angle for the 2nd grating adjusting B.S.1, M.R. 2 and M.R. 3. It is noted that B.S. 3 can not be tuned any more to align the 2nd beam

because any movement of B.S 3 causes its reflected beam, the 1st beam to deviate from the Bragg-matched position for the 1st grating. The alignments of the 5th and 6th beams were carried out following the same procedure as that for the 1st beam and 2nd beam. The adjustment of B.S.4 and M.R.4 set the 3rd beam to the Bragg-matched position for the 3rd grating. The 3rd beam is considered as reference of the power intensities of the 6 input waves. Neutral density filters were used to equalize the intensity of the beams to the 3rd beam. After the six beams were aligned at the Bragg angles for each grating, two object beams were chosen and the other four input beams were blocked. The diffracted two beams in the direction of the reference wave interfered together. The interference between the diffracted beams produced a fringe pattern in inaccurate alignment. Fig. 21 shows the fringe patterns of every pair of diffracted beams. The interference between two beams proves the path difference of each pair of beams is shorter than the coherence length of the laser. Therefore, after reducing multiple fringe lines to a single fringe, the diffracted beams can be combined using PZT controllers and lock-in amplifiers to lock the beam in phase.

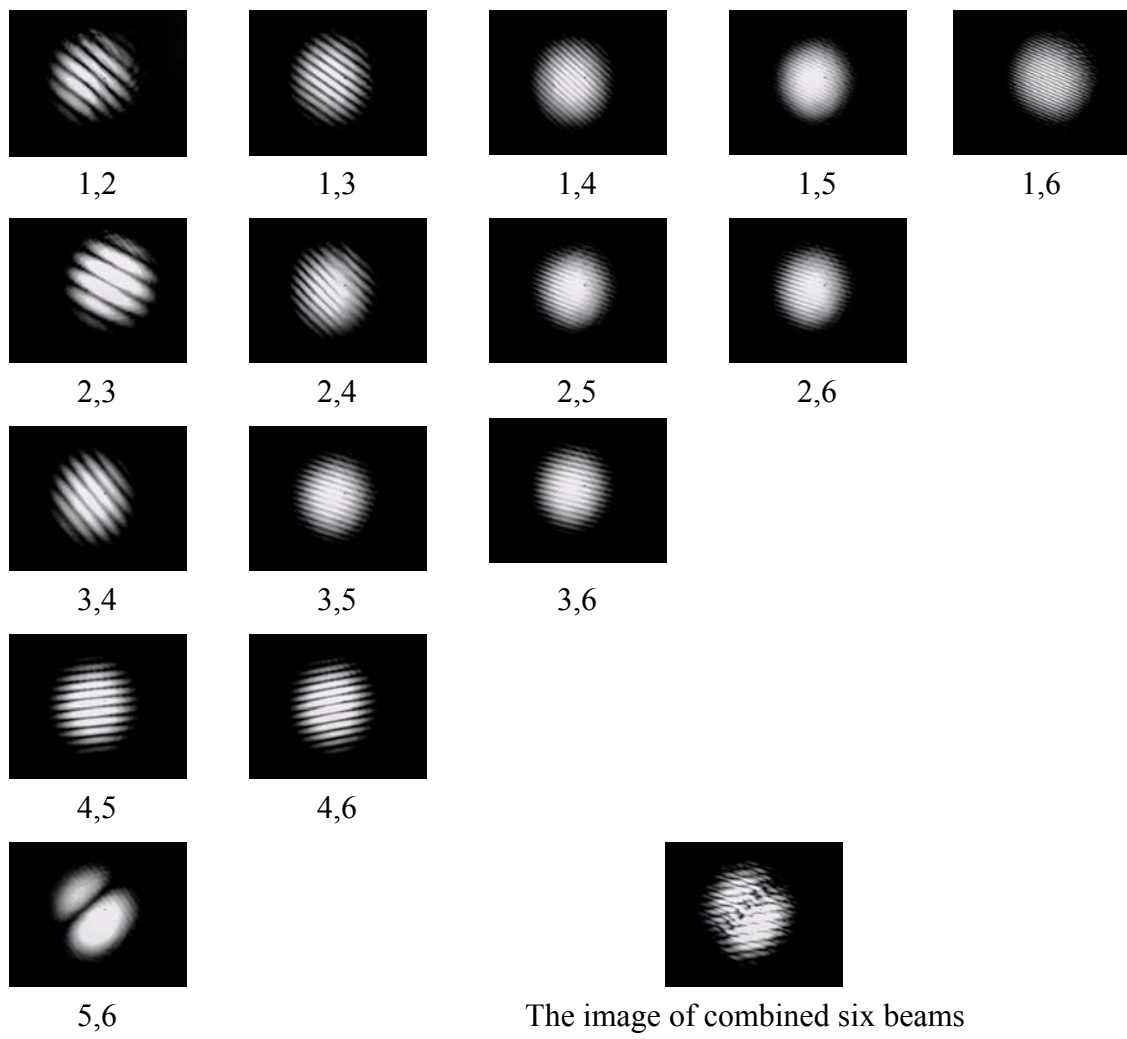
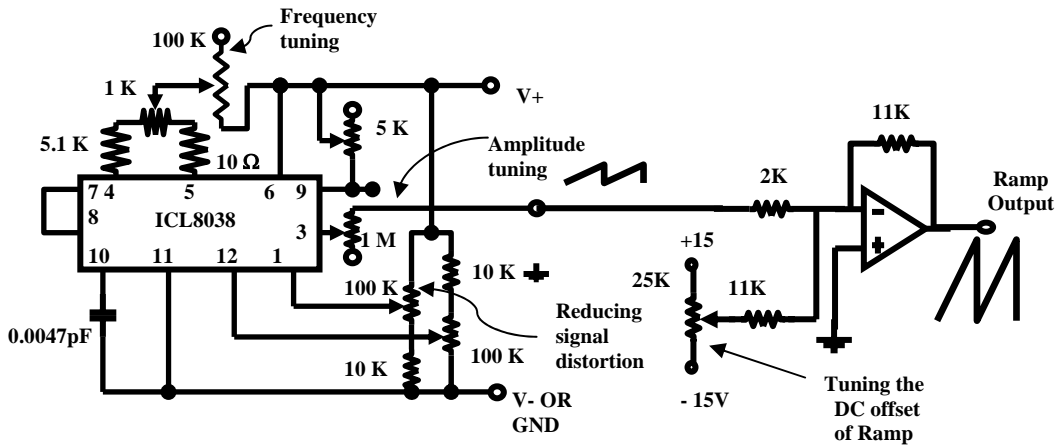


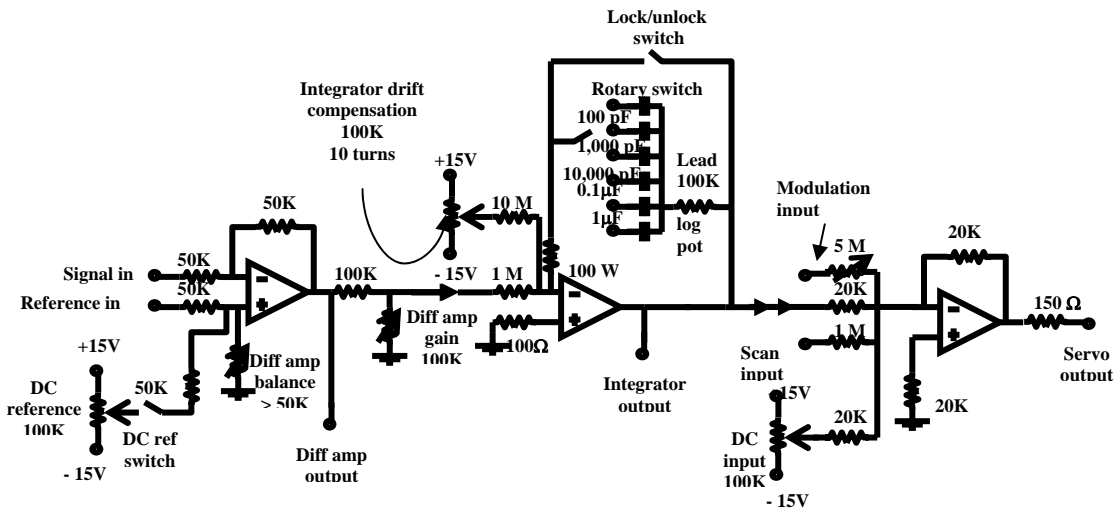
Fig. 21. The fringe patterns by interference of each pair of beams. The number below the images notes the numbers of two input beams.

A ramp generator was implemented using Harris' ICL8038 [4] as shown in Fig 22(a). The two 100K potentiometers which are connected to pin 1 and 12 minimize signal distortion. The ratio of the rising portion to the falling portion of the ramp signal was equal to that of the resistance connected to pin 4 to the resistance connected to pin 5. To accomplish a signal close to an ideal ramp signal, the 1K pot between 5.1K and 10Ω was totally assigned to 5.1K. The frequency was adjusted by a 100K pot which was connected to the 1K pot.

A servo was used to control the system. Figure 22(b) shows a schematic of the servo combined with a summing amplifier. A reference is a desired signal for the system. A differential amplifier compares the input signal with the reference and produces an error signal. An integrator is fed with the error signals and gives a corrected signal which was used to modify the system and accomplish a desired system response. A 50K pot which was connected to the non-inverting input of the differential op-amp, compensated for unbalanced input impedance of the non-ideal op-amp. Integrator drift compensation with a 100K pot provides a dc current to compensate current leakage and prevent the current leakage from saturating the capacitor.



(a) Ramp generator using Harris' ICL8038.



(b) Servo combined with summing amplifier.

Fig. 22. Schematic diagrams of (a) ramp generator and (b) servo

The scan and modulation of the Gaussian profile of the laser intensity at frequency f were carried out by ramp and sine signal as shown Fig. 23(a). Modulated signal whose DC offset is moving along the Gaussian profile, is oscillating at the modulation frequency, f . However, at the peak of resonance, the oscillating frequency becomes doubled because of the symmetry of the Gaussian distribution. Fig. 23(b) shows the modulated Gaussian profile when demodulated and filtered out by the lock-in amplifier. The modulated signal excluding the peak of resonance can be written as

$$V_{\text{modulated}} = \text{D.C.} + \cos(2\pi ft + \theta(V_{\text{PZT}})) \quad (44)$$

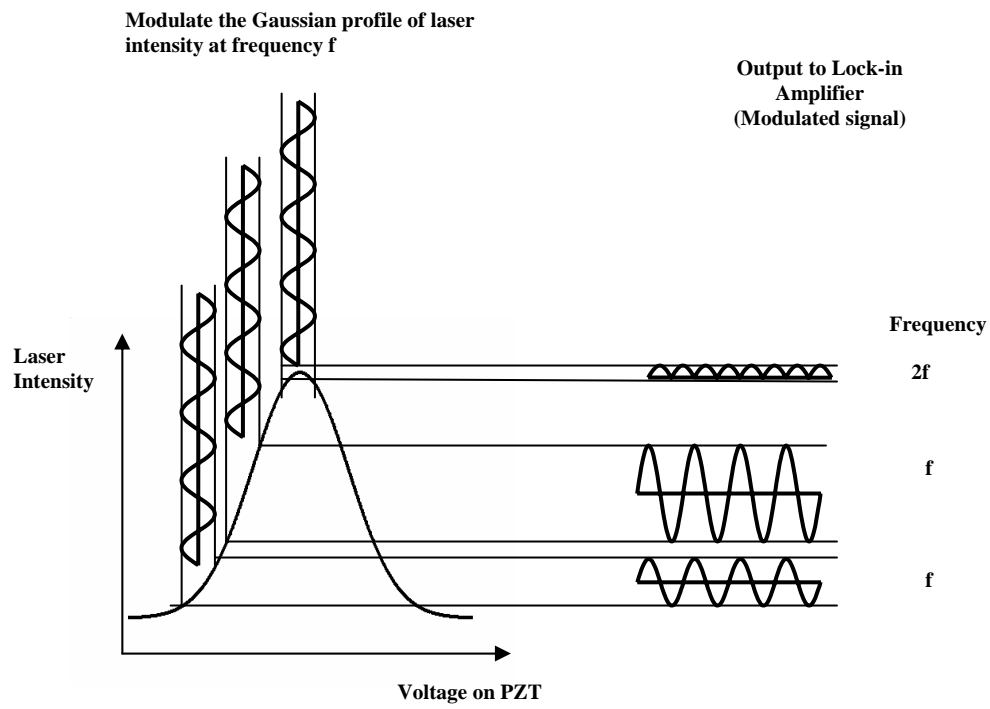
where $V_{\text{modulated}}$ is the voltage of the modulation signal, t is time, D.C. is the D.C offset of the sinusoid whose locus is the Gaussian profiles, θ is the phase delay of the modulated signal with respect to a carrier signal whose frequency is equal to the modulation frequency f . The phase delay can be expressed as a function of the voltage through PZT because the slope of the Gaussian profile varies as the PZT voltage. The modulated signal is demodulated by the carrier signal and can be express by

$$V_{\text{de modulated}} = [\text{D.C.} + \cos(2\pi ft + \theta(V_{\text{PZT}}))] \cos(2\pi ft) \quad (45)$$

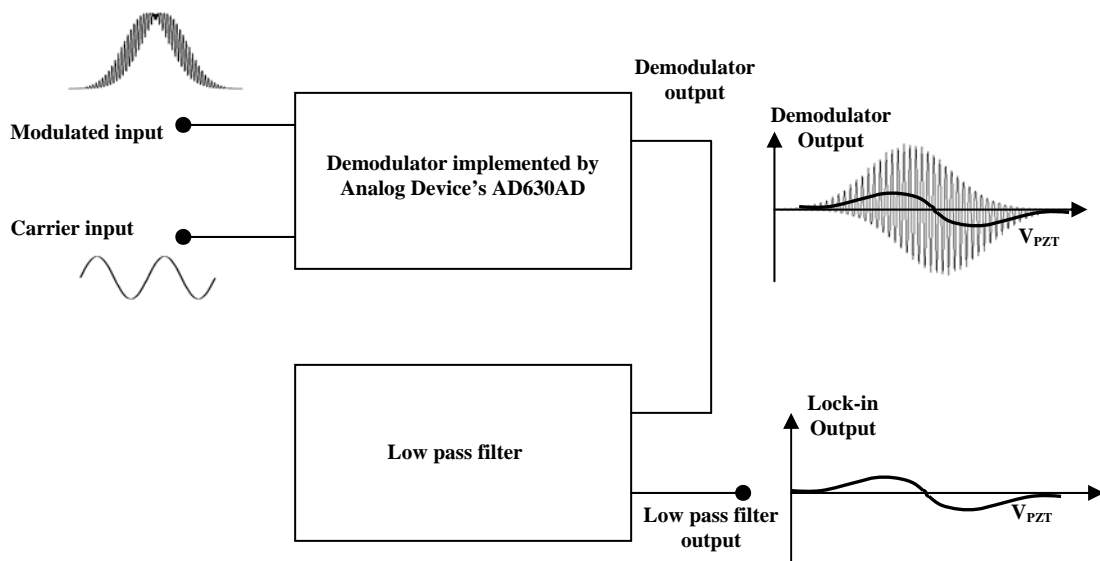
Demodulator in lock-in amplifier is fed with the modulated signal. After the demodulated signal is filtered out by low-pass filter whose cut-off frequency is lower than f , the output of lock-in amplifier is

$$V_{\text{lock-in output}} = 1/2 \cos\theta(V_{\text{PZT}}) \quad (46)$$

At the peak of resonance, the output of lock-in amplifier becomes zero because the frequency of the modulated signal is twice frequency f and the lock-in amplifier can detect signals only at the frequency f . The locus of Eqn. (46) as a function of V_{PZT}



(a)



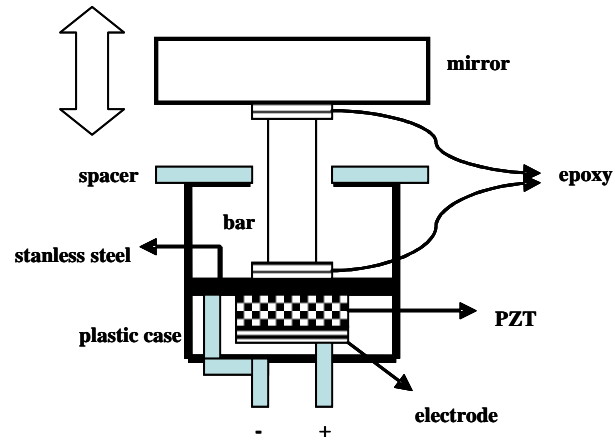
(b)

Fig. 23. Ramp and sinusoid signals scan and modulate laser intensity.

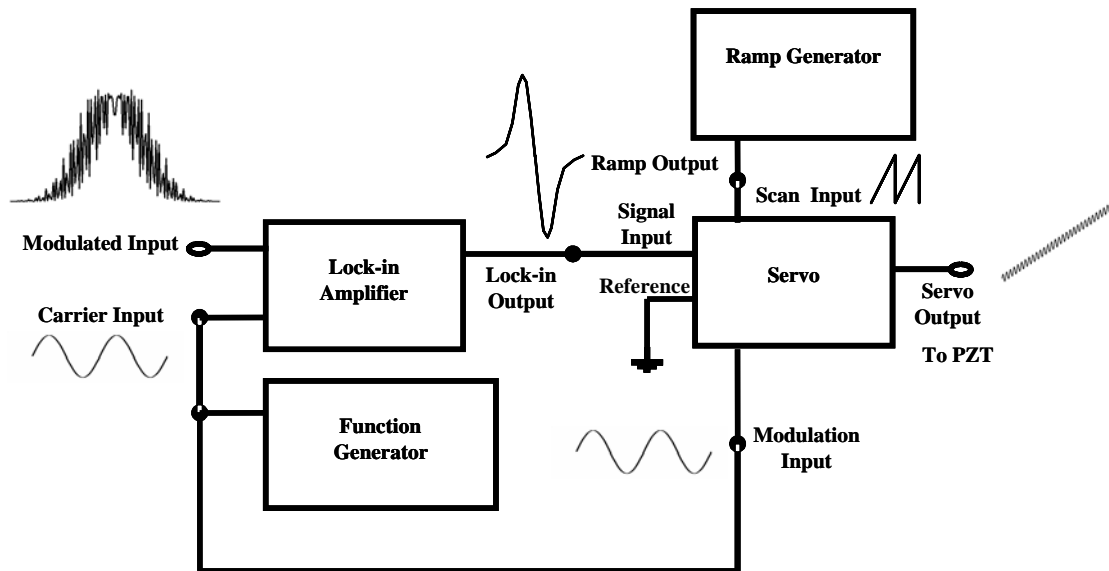
and the behavior of zero-crossing at the resonance peak depict the output of lock-in amplifier as the derivative of the Gaussian profile as shown in Fig. 23(b).

Fig. 24(a) shows the schematic diagram of a mirror mounted on PZT driven by servo output signal. The optical path difference was changed by the movement of mirror caused by the thickness change of PZT. Fig. 24(b), and (c) show the block diagram of an entire PZT controller, and read-out setup to combine six beams respectively. Each input wave was propagating in the direction of each object wave ($S_1 \sim S_6$) and the diffracted wave in the direction of the reference wave (S_0) was illuminating a photodetector as shown in Fig. 24(c). A summing amplifier inside the servo loaded a sinusoid on a ramp signal to drive the PZT and modulate the intensity of a combined pair of beams. Five PZTs were used to lock the phases of five beams to that of the 3rd beam which was chosen as a reference. PZTs resonate at different frequency because the weights of loads on PZTs are not exactly same and this inequality influences on the responses of PZTs. Each pair of beams was modulated at a different frequency which was within the resonant frequency range of each PZT. The modulated signals were detected by one photodetector. Therefore the separation between the modulation frequencies was set to about 100 Hz to identify the modulated signal of each pair of beams and prevent it from mixing with that of other pair of beams. Function generators provided sinusoids used for modulation and demodulation. The modulated signal was applied to a lock-in amplifier to obtain the derivative of the intensity profile of the combined two beams. The reference of a servo was set to zero volts and the servo locked the input signal to zero volts. The function of the lock-in amplifier was to turn the peak of intensity of the

combined two beams into zero. The lock-in output signal was applied to the input of the servo. The zero crossing of the derivative was used to lock the intensity of the combined two beams to the peak. If voltage through PZT deviates from the voltage at which the intensity shows maximum value, the lock-in output becomes non-zero. The differential amplifier of the servo compares the non-zero signal to the reference which was set to zero. The integrator of the servo corrects the detected error signal produced by the differential amplifier. The corrected signal was used to modify the PZT voltage. At the modified voltage, the PZT changed optical path difference between one beam and the 3rd beam. Therefore the pair of beams become in phase and the intensity of combined two beams restored the maximum value. The lock-in output, which was applied to the servo input, returns zero which was the servo reference, i.e. the intensity of two combined beam can stay at peak locking a lock-in output to zero with a servo.

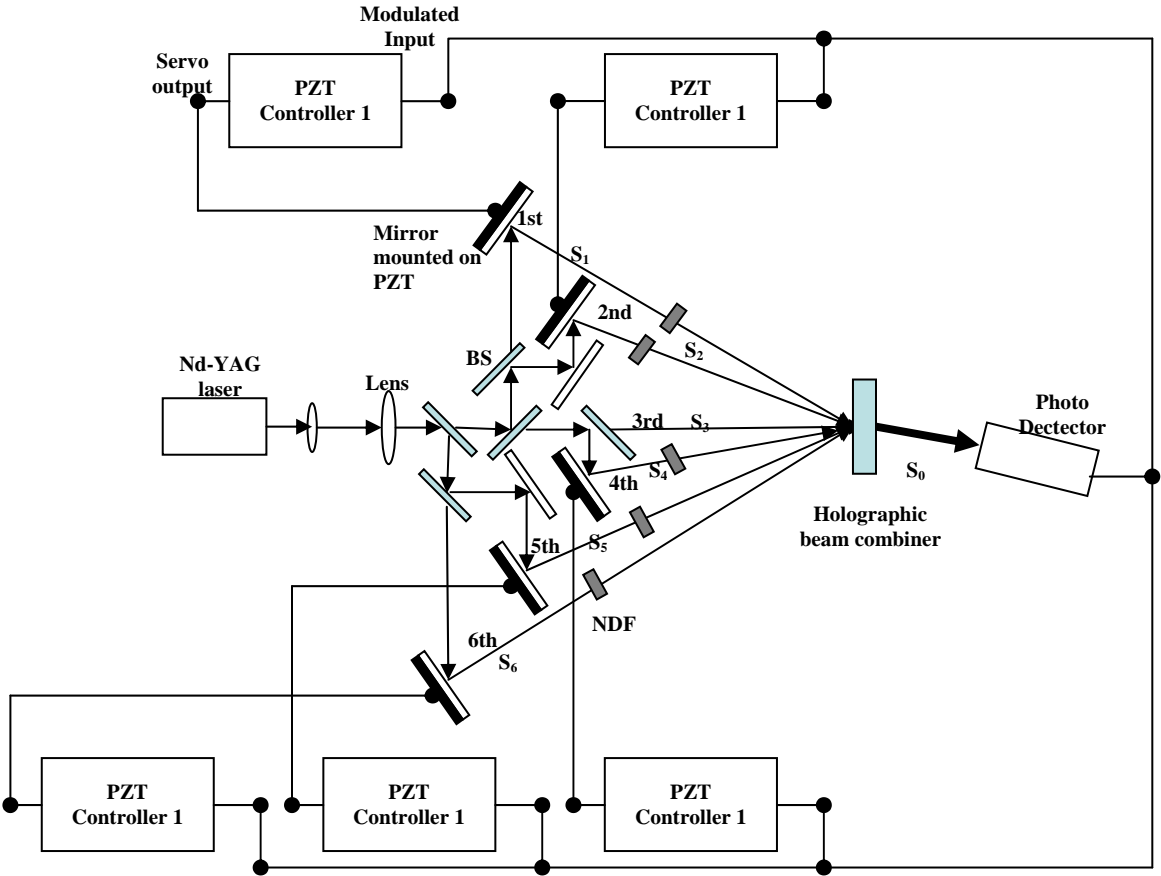


(a) Mirror mounted on Panasonic's Piezoelectric Ceramic Buzzer units, EFB-RD22C415.



(b) Entire PZT controller.

Fig. 24. The PZT controller consists of the circuits in Fig. 19, Fig 21 and Fig. 22, and sine wave function generators. Mirrors were mounted on PZTs driven by ramp generators.



(c) Readout set-up controlled by PZT.

Fig. 24 continued

Table 4(a) and (b) show conditions for the combination of each pair of beams, the intensities of the each input and diffracted wave. The 3rd beam was chosen as a reference. 1.25Hz ramp signal was used to scan the Gaussian profile because the PZT with mirror did not respond at higher frequency. The number of Gaussian profiles was proportional to the amplitude of ramp signal. It was necessary that the amplitude covers the PZT voltage of at least one peak because to lock the intensity of the combined two beams to the maximum value, at least one discriminant from lock-in output applied to the input of servo. The width of the Gaussian profile narrowed as the frequency of the ramp signal increased. As shown in Table 4(b), input waves were not completely diffracted into the direction of reference wave S_0 because the input wave was partially reflected by the surface of the material and the reconstructed wave S_0 was partially diffracted again into the directions of the six objective waves ($S_1 \sim S_6$) before the leaving holographic gratings. Due to difficulty with alignment, the input wave deviated from the center of the hologram. The grating strength, 0.23π at the center of the hologram decreased along the radius of the hologram showing the Gaussian distribution. Therefore, illumination with the center of reading beam on the center of the hologram without deviation resulted in high diffraction efficiency.

The diffracted beam of each input wave is in phase and interfering constructively. The output intensity in the direction of S_0 is the square of the sum of the input waves' electrical fields. Therefore the total intensity of diffracted waves can be written as

$$I_{\text{total}} = \left(\sqrt{I_1} + \sqrt{I_2} + \sqrt{I_3} + \sqrt{I_4} + \sqrt{I_5} + \sqrt{I_6} \right)^2 \quad (47)$$

where I_N ($N=1\sim 6$) is the intensity of the diffracted wave in the direction of reference wave S_0 when each input wave ($S_1\sim S_6$) is incoming separately. The calculated total intensity of combined six beams was 1.26899V and 0.33V was experimentally measured.

Table 4(a). Experimental conditions for the combination of each pair of beams. Scan range and modulation frequency are determined by PZT response. The scan range is wide enough to obtain two or three peaks and the modulation frequency is set within PZT resonance frequency range.

Combined two beams	Modulation Frequency(Hz)	Scan range(V)
Beam 1 & 3	1600	-3 ~7.5
2 & 3	1400	-15~15
3 & 4	600	0~5
3 & 5	1870	-15~15
3 & 6	800	1~7

Table 4(b). The intensity of each input wave is equalized by neutral density filters as shown in Fig. 24(c). The intensity of each diffracted wave is measured by a photodetector.

	S ₁	S ₂	S ₃	S ₄	S ₅	S ₆
Intensity of Input wave(V)	0.5	0.5	0.5	0.5	0.5	0.5
Intensity of Diffracted wave(mV)	30	40	40	35	35	35

**V. BEAM COMBINATION USING PLANO-CONVEX LENS AND
EXPERIMENTAL PERFORMANCE OF THE INJECTION LOCKING FOR
POTENTIAL READING SETUP**

A. Investigation of the Influence of Phase Angle Variation Between Two Input Waves on the Intensity of an Output Wave

We investigated the influence of the variation of phase angle difference between adjacent input waves on the intensity of the output wave for the case that N input waves have equally separated phase angles within one period in the beam combiner mode. S_0 and S_h are the amplitudes of the reference and h_{th} object waves respectively.

A phase angle difference between adjacent input waves is constant. The boundary conditions at $z=0$ for Eqn. (17) are

$$S_0(0)=0, S_1(0)=1, S_2(0)=e^{j\phi}, S_3(0)=e^{j2\phi}, S_4(0)=e^{j3\phi} \dots\dots S_N(0)=e^{j(N-1)\phi}$$

where ϕ is the phase difference between adjacent waves. We obtain the solution of the amplitude of S_0 at $z=d$.

$$S_0(d) = -\frac{1}{2} \sqrt{\frac{\prod_{h=1}^N C_h}{C_0 \gamma}} \left[\sum_{h=1}^N \kappa_h e^{j(h-1)\phi} \right] \left[\exp \left(j \sqrt{\frac{\gamma}{\prod_{h=0}^N C_h}} d \right) - \exp \left(-j \sqrt{\frac{\gamma}{\prod_{h=0}^N C_h}} d \right) \right] \quad (48)$$

$$\text{where } \gamma = \sum_{h=1}^N \left[\frac{\left(\prod_{k=1}^N C_k \right) \kappa_h^2}{C_h} \right]$$

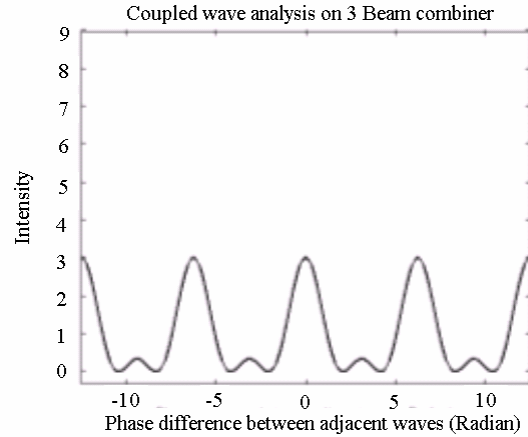
The intensity of output wave, I can be written as

$$I = S_0(d)S_0^*(d) \quad (49)$$

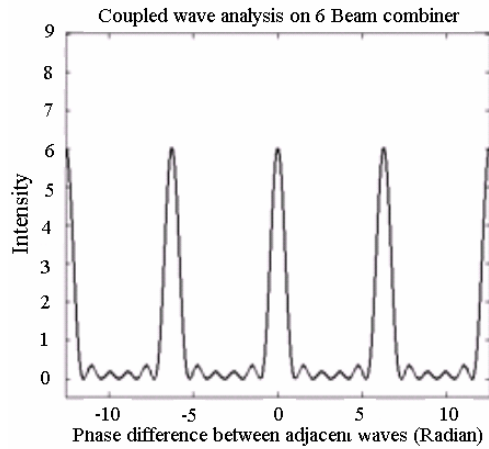
From simulations of the intensity the profiles of an output wave using simulation, it can be assumed that grating strengths for N holograms are equalized to a value at which beam combiner shows maximum diffraction efficiency. Therefore the assumption yields the equalized grating strength for N superimposed holograms as

$$v_1 = v_2 = v_3 = \dots = v_{N-1} = v_N = v = \frac{\pi}{2\sqrt{N}}.$$

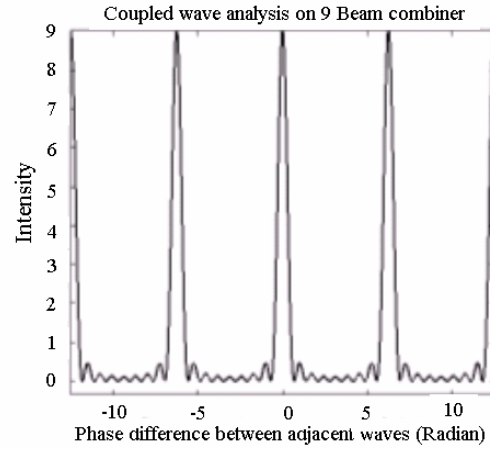
The beam intensities from Eqn. (48) are plotted as a function of phase difference ϕ in Fig. 25(a), (b), (c) for the three cases when 3, 6 and 9 incoming waves respectively, and the grating strengths are equalized at the value of $\frac{\pi}{2\sqrt{N}}$. In the three cases, in-phase input waves are completely combined and the intensities reach maximum value which is equal to the sum of the intensity of individual unit input waves. Fig.25(a), (b), (c) show the finesse corresponds to the number of input waves and the half-width shrinks as the number of input waves increases. The finesses of a 6 and 9 beam combiner are double and triple that of 3 beam combiner respectively.



(a) 3 input waves



(b) 6 input waves



(c) 9 input waves

Fig. 25. Calculated intensity of output wave in the direction of reference wave S_0 as a function of phase angle between adjacent input waves. Every input wave has unit intensity. (a) $N=3$, $v=\frac{\pi}{2\sqrt{3}}$ in Eqn. (48); (b) $N=6$, $v=\frac{\pi}{2\sqrt{6}}$ in Eqn. (48); (c) $N=9$,

$v=\frac{\pi}{2\sqrt{9}}$ in Eqn. (48).

In Fig. 26(a) the output intensity of a 6 beam combiner is plotted as a function of equalized grating strength when the all input waves are in phase. Fig. 26(b) shows the output intensity as a function of phase angle between adjacent waves when the equalized grating strength is set to the three values of ν for output intensities 2, 4 and 6 as represented in Fig. 26(a). The height of the peak decreases as the grating strength reduces to the value of 0.2500 which is expected from Fig. 26(a). The finesses of three peaks have the same value of 6.

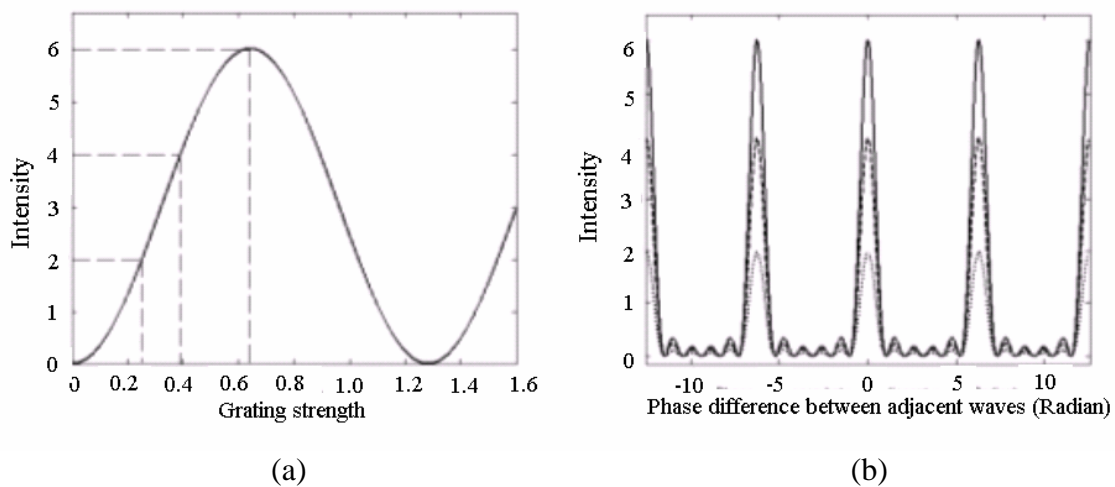


Fig. 26. (a) Simulation results showing the intensity of the output wave as a function of equalized grating strength, ν . Six input waves have unit intensity and are in-phase. Therefore, ϕ is set to 0 in Eqn. (48). (b) Simulation result showing the intensity of the output wave as a function of phase angle between adjacent waves for three values of ν . Solid line for $\nu=0.6409$, dashed line for $\nu=0.3850$, and dot line for $\nu=0.2500$ in Eqn. (48).

B. Experimental Demonstration of 6 Beam Combiner Varying Phase Angle Between Adjacent Waves

Fig. 27 shows the result when the boundary conditions at $z=0$ are the same as assumed for the simulations in Fig. 25, and the grating strength is equalized to that of holograms within the second sample, 0.23π in Table 3 of Section III. The second sample has six holograms which show uniform diffraction efficiencies.

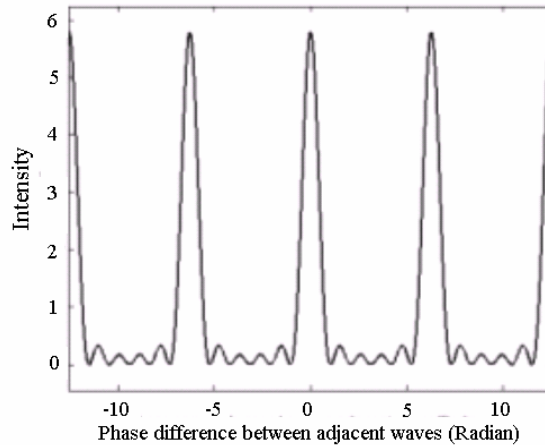


Fig. 27. The intensity of S_0 is plotted as a function of phase angle difference between adjacent waves for $\nu=0.23\pi$.

As shown in Fig. 27 it is determined that 6 beams can not be completely combined with the beam combiner, which is realized by the second sample, and the simulation predicts that peak maximum height that can be experimentally obtained is 5.8.

The combination of six waves was performed with the second sample. Fig. 28 describes the experimental set-up using plano-convex lens. The input wave from a Nd-

YAG laser illuminates the holograms in the direction of the reference S_0 and split into six waves. The waves represented by solid lines are propagating in the beam splitter mode. The flat surface of the lens faces the holograms which is the point source of the split six waves. Therefore both surfaces contribute to refractions to minimize spherical aberrations. The six waves are paralleled by the lens and reflected by a mirror. The incident angle displacement between adjacent object waves is constant during hologram recording. Therefore the phase angles of the six diffracted waves can be distributed with equal separation ϕ . The six reflected waves illuminate the holograms in the beam combiner mode. The combined beam was partially reflected by a beam splitter. The partially reflected beam is monitored by a photo detector and the mirror was adjusted to vary the phase angle difference. The waves represented by dashed lines are propagating in the beam combiner mode.

The sum of the intensity of the individual split beams is defined as $6I_0$ measured as 760mV after the splitter but before the lens in Fig. 28. I_0 notes the average intensity of each individual beam. At this point, the undeflected beam was measured as 20mV. The results of Fig. 27 show that the maximum peak height which can be theoretically obtained by our holographic beam combiner is 734 mV. Fig. 29 shows the intensity of the partially reflected combined beam measured by a photodetector. It is noted from the 3rd and 4th peak on the left, that the half width covers 0.7 fractional divisions in one rectangular box and the distance between peaks is 4 fractional divisions. The measurement yields the finesse of a 6 beam combiner as 5.7 which is approximately equal to the value theoretically estimated. We can confirm that all six input waves

contribute to beam combining. The height of the highest peak was measured to be 265mV at the detector in Fig. 29. The beam splitter (B.S) in Fig. 28 reflects 61.54%. Therefore the intensity of the combined beam is calculated as 475.6mV corrected for reflection from hologram surface. The experimental output is lower than the theoretically expected output of 734mV.

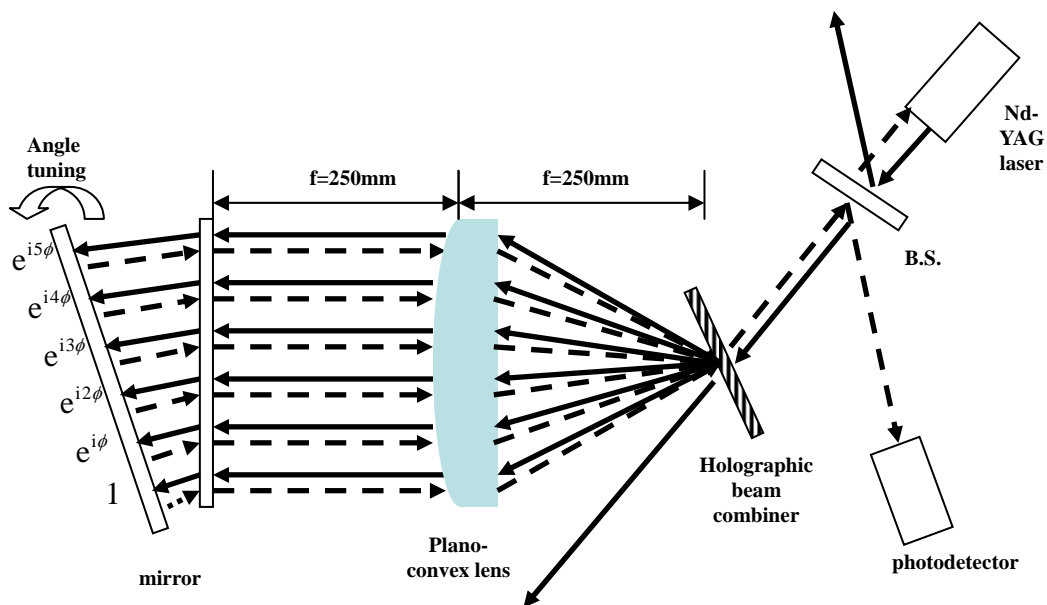


Fig. 28. Experimental setup for six beam combining with the 2nd sample which has six superimposed gratings and functions as holographic beam combiner. The focal length of lens is 25cm.

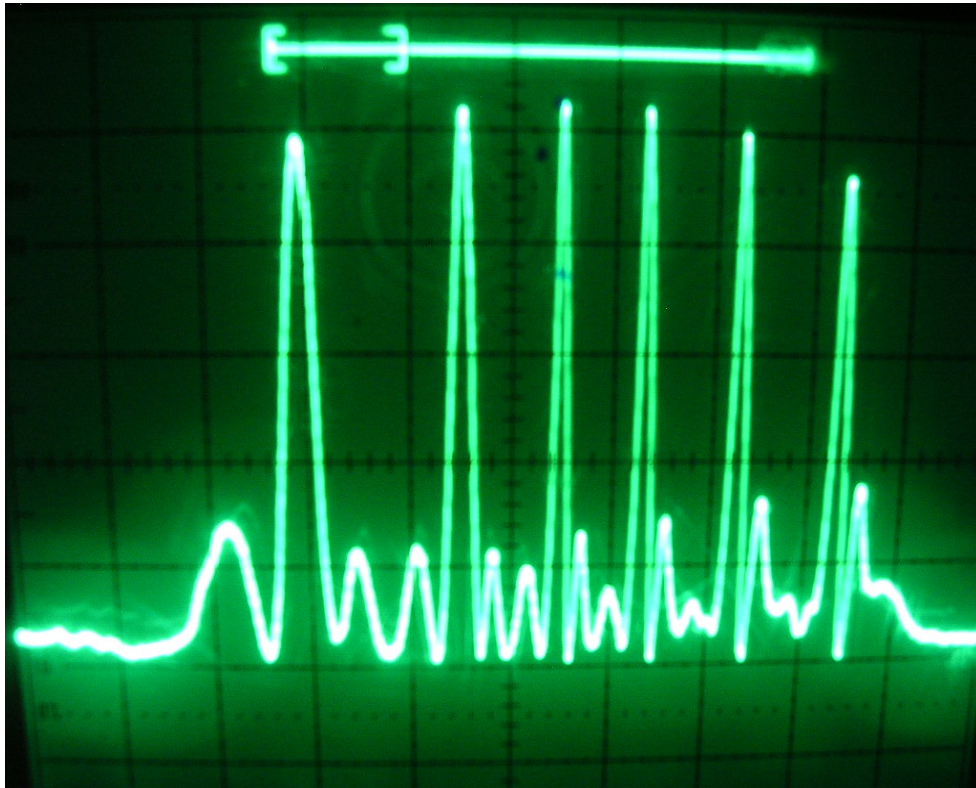


Fig. 29. Intensity measured by photodetector in experimental setup as shown Fig 28. One longitudinal division of rectangular box is 50 mV. One lateral division is 0.1s. The D.C offset of photodetector is -100 mV.

The cause of the degradation in the efficiency of a holographic beam combiner can be explained by the following: the input waves were not completely diffracted in the direction of reference wave S_0 because the reconstructed wave S_0 was partially diffracted again in the directions of the six objective waves ($S_1 \sim S_6$) before leaving the holographic gratings. Due to alignment difficulty, the location of the input wave deviated from the center of the hologram. The grating strength, 0.23π at the center of the hologram degenerates along the radius of the hologram showing the Gaussian distribution. Therefore, illumination with the center of reading beam on the center of the hologram

without deviation results in high diffraction efficiency. The error of angle displacement during holographic recording can bring about phase angle difference variation between adjacent beams. Since that, phase angle mismatch always exists. All input beams can neither be in-phase simultaneously nor fully combined.

C. Frequency Synchronization of Diode Lasers by Injection Locking

Laser diodes are more sensitive to injected light than normal lasers due to the small number of photons inside the laser cavity. Optical feedback can be used to synchronize the frequency of a slave laser to a master laser. The light from the master laser is injected into the slave laser. We present an experimental investigation of injection locking of semiconductor lasers. Fig. 30 shows the experimental set-up. The faraday isolator (FI) is positioned between the master laser (ML) and slave laser (SL) to provide an one-way path from the ML to the SL. The polarization axis of the ML is rotated by the IS. The half wave plate again rotates the polarization axis of the ML. Therefore the direction corresponds to the direction of the polarization axis of the SL to maximize the feedback effect on the SL. A CCD camera captures the image of the combined two beams. The observance of fringe patterns in the image confirms that two light sources become coherent.

Fig. 31(a) shows the image taken by the CCD camera when the optical feedback from the ML is blocked. The fringe patterns disappear because the SL is not lock to the ML and freely runs without the feedback. Fig. 31(b) shows the fringe patterns caused by the optical feedback.

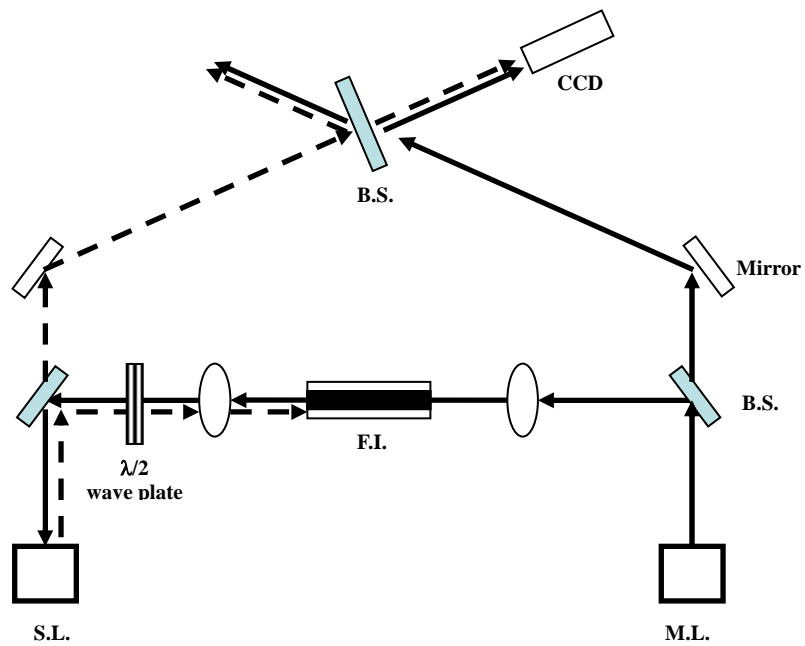


Fig. 30. Combined set-up for a two beam interferometer and injection locking. ML: master laser, SL: slave laser, FI: faraday isolator, Solid line: Injected beam into slave lasers, Dashed line: beam from slave lasers.

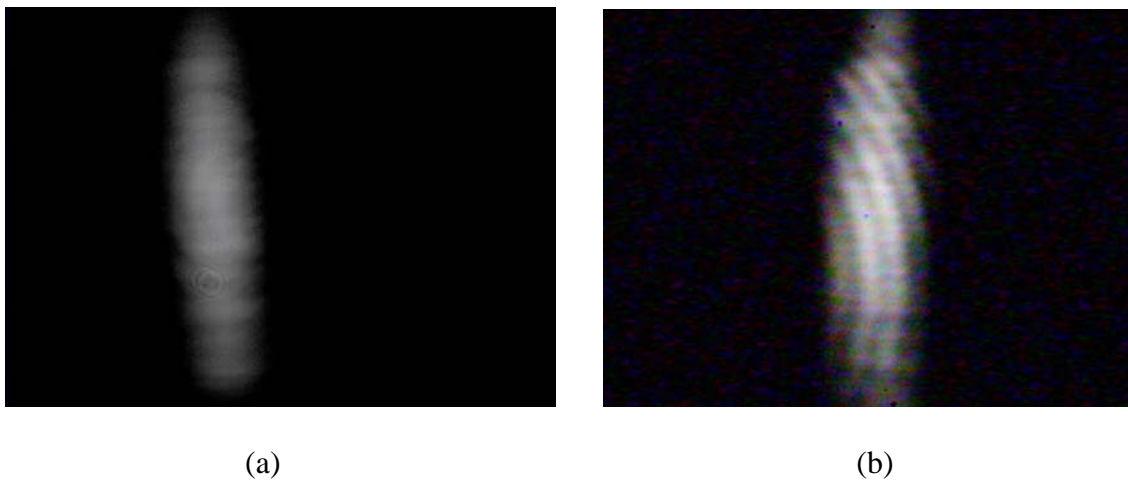


Fig. 31. Image of the combined two beams captured by a CCD (a) without and (b) with optical feedback.

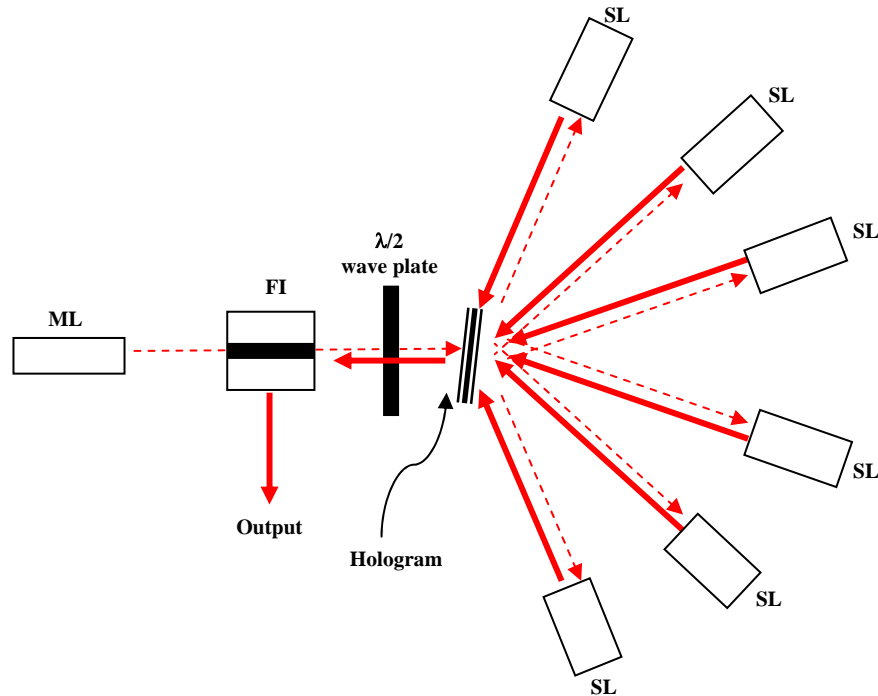


Fig. 32. Expected read-out setup using injection locking ML: master laser, SL: slave laser, FI: faraday isolator, Dashed line: Injected beams into slave lasers, Solid line: Coherent input beams from slave lasers.

Injection locking is used to obtain six coherent light sources as shown in Fig. 32. The beam from the ML illuminates the holograms at the common Bragg angle and split into six beams. The split beams are injected into the six SLs. The frequencies of the six SLs are synchronized to that of the ML. Consequently, six SLs behave as six coherent sources. The six input beams from the SLs propagate along the optical paths which are identical to those of the six split beams and illuminate the holograms in the beam combiner mode.

VI. CONCLUSIONS AND FUTURE WORK

A six beam combiner can be used to obtain high power lasers by combining inexpensive low power lasers. In this study, we have performed a six beam combination using six superimposed holographic gratings recorded in the same spatial location.

The coupled equations for N superimposed holograms were expanded to explain wave propagations within lossless or lossy media and on the Bragg-matched or Bragg mismatched conditions. The simulated results presented herein showed the diffraction efficiencies as a function of the equalized grating strength for four different boundary conditions. The theoretical analysis guided the choice of an equalized grating strength at which the six beams could be completely combined or split. The diffraction efficiencies were found to oscillate periodically. Therefore an equalized grating strength for maximum diffraction efficiency could be chosen within the dynamic range of a holographic material. The simulated results showed that the six beams were fully combined by holographic gratings with the equalized grating strength $0.204\pi+0.408N\pi$ (N is zero or positive integer).

Six holographic gratings were recorded by angular multiplexing. The exposure time for a unit diffraction single grating was measured as 8s. But theory requires the equalized grating strength of 0.204π . Therefore, the exposure time of the 1st grating reduced to 4s, and the exposure times from the 2nd to 6th grating decreased with order of exposure in order to acquire balanced diffraction efficiencies. Equalized grating strengths for two different groups of holograms recorded with different exposure schedules were determined by the readout of holograms in the beam splitter mode, and

by comparing the simulated results with the experimentally observed ring pattern in transmitted and diffracted beams with simulation results. Using this method, one could predict the exposure schedule for recording N holograms with equalized grating strength which is required for a uniform high diffraction efficiency beam combiner.

Using lock-in amplifiers, oscillators, ramp generators and servos, the phases of five beams were locked to the phase of a reference which was chosen from one of the six input beams, and six beams combination was attempted. The intensity of each combined pair of beams was modulated at a different frequency which was determined by a PZT response. The lock-in process produced the derivative of the sinusoidal profiles of the intensity and the peak intensity was changed to zero-crossing. The servo locked to the zero crossing. Consequently the D.C voltage of PZT was adjusted by the servo output to lock the intensity to the peak. The intensity of a six beam combiner was measured experimentally and was found to be much lower than the sum of the intensities of the six input beams.

A simplified method to characterize the beam combiner was performed with plano-convex lens and mirrors. A single laser source was split into six copies while maintaining the optical path difference shorter than the coherence length. The six beams were made parallel by the plano-convex lens and reflected by a mirror. In order to minimize spherical aberration, the flat surface of the lens faced the holographic beam combiner. The mirror was adjusted to vary the phase angle between adjacent beams. The reflected beams were converged by the lens back into the hologram with the correct alignment to recombine. The intensity of the combined beam was monitored by a

photodetector. Simulation results showed that the intensity plotted as a function of the phase angle was similar to the intensity profile for the case of multiple reflections in an etalon. The finesse was equal to the number of input beams. However, the height of the peak was equivalent to the output intensity which could be obtained by the assigning equalized grating strength to each hologram. It was theoretically determined that our six holograms with an equalized grating strength of 0.23π yielded, a height of peak of 734mV when the total input intensity was 760mV. The experimentally measured intensity was 475.6mV, which is 64% of expected or 62% of the perfect beam combiner.

Multiple coherent light sources are indispensable in order to realize a beam combiner. The coherent light sources can be accomplished by injection locking. In the experimental demonstration of injection locking, a single slave diode laser was locked to one reference laser diode. Fringe patterns in the image of two combined beams confirmed that the two independent diode lasers behave coherently.

Many researchers have investigated the frequency synchronization of one or several diode lasers to one reference diode laser by injection locking [5][6][7]. This method is potentially another technique for the combination of multiple input waves. An experimental set-up for future research was proposed using injection locking to accomplish six coherent light sources. In our experiment, the reference diode laser illuminates six holograms at the common Bragg angle. The reference beam is split into six beams which are injected into the cavities of six laser diodes in order to synchronize the laser diodes to the reference. The output waves from the six laser diodes propagate back along the same path as the injected beams and, illuminate the holographic beam

combiner. It is expected that six coherent light sources are obtained and one can be combined without the complicated PZT controller systems.

M/# is an important factor which determines how many holograms can be recorded with given grating strength and desired diffraction efficiency. The M/# of the dye doped photopolymer was determined by the analysis of a multiple-ring diffracted beam which was much simpler than the conventional technique which requiring the recording of many holograms. In the conventional measurement, 1000 hologram were recorded on the same spatial location. However, in our approach, a single hologram was recorded on the material with an exposure time that was long enough for the grating strength at the center of the recording beam and to reach the limit of the dynamic range. The material was baked until the number of rings reached maximum. The M/# of the material was evaluated by counting the number of the rings in the diffracted beam and observing the brightness on the center rings. The M/# of the dye doped photopolymer was evaluated as 9.42.

REFERENCES

- [1] H. Kogelnik, "Coupled wave theory for thick holographic gratings," *Bell Syst. Tech. J.*, vol. 48, pp. 2909-2947, 1969.
- [2] *What is a Lock-in Amplifier?*, Technical Note TN1000 vol.2.1, Oak Ridge, TN: PerkinElmer, Apr. 2000.
- [3] *AD630: Balanced Modulator/Demodulator Data Sheet*, Norwood, MA: Analog Devices, Jul. 2001.
- [4] *ICL8038: Precision Waveform Generator/ Voltage Controlled Oscillator*, File No. 2864.2, Port Jefferson Station, NY: Harris Semiconductor, Nov. 1996.
- [5] F. Mogensen, H. Olesen, and G. Jacobsen, "Locking conditions and stability properties for a semiconductor laser with external light injection," *IEEE J. Quan. Electro.* vol. 21, no. 7, pp. 784-793, 1985.
- [6] P. Laurent, A. Clairon, and C. Breant, "Frequency noise analysis of optically self-locked diode lasers," *IEEE J. Quan. Electro.* vol. 25 no. 6, pp. 1131-1142, Jun. 1989.
- [7] J. P. Bouyer and C. Breant "Stability of an injection-locked DFB 1.5 μ m semiconductor laser," *J. De Physique* .,vol. 2, no. 9, pp. 1623-1644, Sep. 1992.
- [8] F. H. Mok, G. W. Burr, and D. Psaltis, "A system metric for holographic memory systems," *Opt. Lett.*, vol. 21, pp. 896-899, 1996.
- [9] M. S. Shahriar, J. Riccobono, M. Kleinschmit, and J.T. Shen, "Coherent and incoherent beam combination using thick holographic substrates," *Opt. Commun.*, vol. 220, pp. 75-83, 2003.

- [10] M.-P. Bernal, H. Coufal, R. K. Grygier, J. A. Hoffnagle, C. M. Jefferson, R. M. Macfarlane, R. M. Shelby, G. T. Sincerbox, P. Wimmer, and G. Wittman, "A precision tester for studies of holographic optical storage materials and recording physics," *Appl. Opt.*, vol.35, pp. 2360-2374, 1996.
- [11] L. Solymar, D. J. Webb, A. Grunnet-Jepson, and W. Solymar, *Oxford Series in Optical and Imaging Sciences: The Physics and Applications of Photorefractive Materials*. New York: Oxford University Press, Aug. 1996.
- [12] L. Dhar, A. Hale, H. Katz, M. L. Schilling, M. G. Schnoes, and F. G. Schilling, "Recording media that exhibit high dynamic range for digital holographic data storage," *Opt. Lett.*, vol.24, no.7, pp. 487-489, 1999.
- [13] G. W. Burr, W.-C Chou, M.A. Neifeld, H. Coufal, J. A. Hoffnagle, and C. M. Jefferson, "Experimental evaluation of user capacity in holographic data-storage systems," *Appl. Opt.*, vol. 37, no. 23, pp. 5431-5443, 1998.
- [14] D. Psaltis, D. Brady, and K. Wagner, "Adaptive optical networks using photorefractive crystals," *Appl. Opt.*, vol. 27, pp. 1752-1759, 1988.
- [15] S. K. Case, "Coupled wave theory for multiply exposed thick holographic gratings," *J. Opt. Soc. Am.*, vol. 65, pp. 724-729, 1975
- [16] R. Magnusson, and T. K. Gaylord, "Analysis of multiwave diffraction of thick gratings," *J. Opt. Soc. Am.*, vol. 67, pp. 1165-1170, 1977
- [17] J. Zhao, P. Yeh, M. Khoshnevisan , and I . McMichael, "Diffraction properties of vector synthetic volume index gratings," *J. Opt. Soc. Am. B*, vol. 17, pp. 898-903, 2000.

- [18] J. Zhao, X. Shen, and Y. Xia, "Beam splitting, combining, and cross coupling through multiple superimposed volume-index gratings," *Opt. & Las. Tech.*, vol. 33, pp. 23-28, 2001
- [19] H. Kobolla, J. Schmidt, J. T. Sheridan, N. Streibl and R. Völkel, "Holographic optical beam splitters in dichromated gelatin," *J. Mod. Optic*, vol. 39, no.4, pp. 881-887, Apr. 1992
- [20] L. Solymar and D. J. Cooke, *Volume Holography and Volume Gratings: Multiple Gratings*. London, U.K.: Academic Press, 208-226, 1981.
- [21] R. Burzynski, D. N. Kumar, S. Ghosal, and D. R. Tyczka, "Holographic recording material," U.S. Patent, No. 6,344,297, 2002.
- [22] H. J. Coufal, D. Psaltis, and G. T. Sincerbox, *Holographic Data Storage: Photopolymer Systems*. Berlin, Germany: Springer, 171-195, 2000.
- [23] K. Y. Hsu, S. H. Lin, Y. N. Hsiao, and W. T. Whang, "Experimental characterization of phenanthrenequinone-doped poly(methyl methacrylate) photopolymer for volume holographic storage," *Opt. Eng.*, vol. 42, no. 5, pp. 1390-1396, May 2003.
- [24] A. Pu, K. Curtis, and D. Psaltis, "Exposure schedule for multiplexing holograms in photopolymer films," *Opt. Eng.*, vol. 35, no. 10, pp. 2824-2829, Oct. 1996.
- [25] E. S. Maniloff, and K. M. Johnson, "Maximized photorefractive holographic storage," *J. Appl. Phys.*, vol. 70, no. 9, pp. 4702-4707, Nov. 1991.
- [26] E. N. Leith, A. Kozma, J. Upatmieks, J. Marks, and N. Massey, "Holographic data storage in three-dimensional media," *Appl. Opt.*, vol. 5, no. 8, pp. 1303-1311, 1966.

- [27] D. L. Staebler, J. J. Amodei, and W. Philips, "Multiple storage of thick holograms in LiNbO_3 ," *VII International Quantum Electronics Conference*, Montreal, pp. 611, 1972.

VITA

Ho Nam Yum completed his Master of Science degree at Texas A&M University in August 2004. He received the Bachelor of Science degree in Ceramic Engineering at Yonsei University, Korea in 2000.

His permanent address is 121-1101 Hyundai Apt, Apkujundong, Kangnamgu, Seoul, Korea 135-110